

Article

Design, Synthesis and Structure—Activity Relationships of Phenylalanine-Containing Peptidomimetics as Novel HIV-1 Capsid Binders Based on Ugi Four-Component Reaction

Xiangkai Ji ¹, Jing Li ¹, Prem Prakash Sharma ², Xiangyi Jiang ¹, Brijesh Rathi ² , Zhen Gao ¹, Lide Hu ¹, Dongwei Kang ^{1,3} , Erik De Clercq ⁴ , Simon Cocklin ⁵ , Chuanfeng Liu ¹, Christophe Pannecouque ^{4,*}, Alexej Dick ^{5,*} , Xinyong Liu ^{1,3,*}  and Peng Zhan ^{1,3,*}

¹ Department of Medicinal Chemistry, Key Laboratory of Chemical Biology (Ministry of Education), School of Pharmaceutical Sciences, Cheeloo College of Medicine, Shandong University, 44 West Culture Road, Jinan 250012, China

² Laboratory for Translational Chemistry and Drug Discovery, Department of Chemistry, Hansraj College, University of Delhi, Delhi 110007, India

³ China-Belgium Collaborative Research Center for Innovative Antiviral Drugs of Shandong Province, 44 West Culture Road, Jinan 250012, China

⁴ Laboratory of Virology and Chemotherapy, Rega Institute for Medical Research, K.U. Leuven, Herestraat 49 Postbus 1043 (09.A097), B-3000 Leuven, Belgium

⁵ Department of Biochemistry & Molecular Biology, Drexel University College of Medicine, Philadelphia, PA 19104, USA

* Correspondence: christophe.pannecouque@rega.kuleuven.be (C.P.); ad3474@drexel.edu (A.D.); xinyongli@sdu.edu.cn (X.L.); zhanpeng1982@sdu.edu.cn (P.Z.)



Citation: Ji, X.; Li, J.; Sharma, P.P.; Jiang, X.; Rathi, B.; Gao, Z.; Hu, L.; Kang, D.; De Clercq, E.; Cocklin, S.; et al. Design, Synthesis and Structure—Activity Relationships of Phenylalanine-Containing Peptidomimetics as Novel HIV-1 Capsid Binders Based on Ugi Four-Component Reaction. *Molecules* **2022**, *27*, 5995. <https://doi.org/10.3390/molecules27185995>

Academic Editor: Mourad Elhabiri

Received: 18 August 2022

Accepted: 10 September 2022

Published: 14 September 2022

Publisher's Note: MDPI stays neutral with regard to jurisdictional claims in published maps and institutional affiliations.



Copyright: © 2022 by the authors. Licensee MDPI, Basel, Switzerland. This article is an open access article distributed under the terms and conditions of the Creative Commons Attribution (CC BY) license (<https://creativecommons.org/licenses/by/4.0/>).

Abstract: As a key structural protein, HIV capsid (CA) protein plays multiple roles in the HIV life cycle, and is considered a promising target for anti-HIV treatment. Based on the structural information of CA modulator PF-74 bound to HIV-1 CA hexamer, 18 novel phenylalanine derivatives were synthesized via the Ugi four-component reaction. In vitro anti-HIV activity assays showed that most compounds exhibited low-micromolar-inhibitory potency against HIV. Among them, compound I-19 exhibited the best anti-HIV-1 activity ($EC_{50} = 2.53 \pm 0.84 \mu\text{M}$, $CC_{50} = 107.61 \pm 27.43 \mu\text{M}$). In addition, I-14 displayed excellent HIV-2 inhibitory activity ($EC_{50} = 2.30 \pm 0.11 \mu\text{M}$, $CC_{50} > 189.32 \mu\text{M}$) with relatively low cytotoxicity, being more potent than that of the approved drug nevirapine ($EC_{50} > 15.02 \mu\text{M}$, $CC_{50} > 15.2 \mu\text{M}$). Additionally, surface plasmon resonance (SPR) binding assays demonstrated direct binding to the HIV CA protein. Moreover, molecular docking and molecular dynamics simulations provided additional information on the binding mode of I-19 to HIV-1 CA. In summary, we further explored the structure—activity relationships (SARs) and selectivity of anti-HIV-1/HIV-2 of PF-74 derivatives, which is conducive to discovering efficient anti-HIV drugs.

Keywords: HIV-1; capsid modulators; peptidomimetics; Ugi four-component reaction; drug design

1. Introduction

Human immunodeficiency virus (HIV) is the causal agent of acquired immunodeficiency syndrome (AIDS) that poses a serious threat to global public health [1]. HIV consists of two genotypes, HIV-1 and HIV-2. HIV-1 is more virulent than HIV-2, and is mainly responsible for the major pandemic worldwide. However, the increasing risk of HIV-2 infection should also be taken seriously [2]. Combined antiretroviral therapy (cART) has been an effective method for anti-AIDS treatment in the past decades, transforming AIDS into a controllable chronic disease and successfully prolonging patients' lives. However, long-term use of cART programs suffers from many risks, such as drug resistance, drug-drug interactions, severe toxicity, and other adverse reactions [3]. Therefore, there is still an urgent need to identify novel therapies for antiretroviral drugs and novel and unexplored

mechanisms of action to achieve a cure for HIV infection. HIV capsid (CA) is an asymmetric fullerene-shaped cone comprised of about 1500 CA monomers. This cone-shaped lattice consists of approximately 250 hexamers and 12 pentamers [4]. CA monomer can be divided into the N-terminal domain (NTD) and C-terminal domain (CTD), which are connected by a flexible linker [5]. In the early stage of viral replication, the capsid proteins can interact with the host factors, such as nucleoporin 153 (NUP153), cleavage, and polyadenylation specificity factor-6 (CPSF6), to complete the uncoating process and help to complete the reverse transcription, nuclear import, and integration process [6]. In the late stage of viral replication, capsid proteins assemble into the recombinant capsid, encapsulating viral RNA and gag-pol precursor proteins. In addition, capsid proteins can also evade the immune system by interacting with numerous host factors [7,8]. Therefore, the capsid protein is a promising target for anti-HIV drug design and development due to its critical functions within the viral life cycle [9–11].

Numerous antivirals targeting HIV have been reported [12–18]. **PF-74** (1, Figure 1a), as the first small molecule cocrystallized with the HIV-1 CA protein, has received the most extensive attention and research [19]. During the early stage of HIV replication, **PF-74** can competitively, with host factors CPSF6 and NUP153, interact with HIV-1 CA, interfering with numerous viral processes, including viral uncoating, reverse transcription, nuclear import, and integration [7,8]. At a later stage, it adversely affects the stability of capsid and viral maturation by interfering with the normal late-stage CA assembly process [6]. However, its clinical application has been limited because of moderate activity ($EC_{50} = 0.52\text{--}0.90\ \mu\text{M}$), a poor drug-like profile, and poor metabolic stability ($T_{1/2} = 0.5\text{--}1.3\ \text{min}$) [17,20–22]. **GS-6207**, a **PF-74** derivative developed by Gilead Sciences and currently in phase III clinical trials, shows an increased affinity for CA by adding multiple hydrogen bond donors and acceptors. However, its clinical application is limited by its complex synthetic route, administration mode, and drug resistance [22–24].

Structural studies showed that the phenylalanine core of **PF-74** formed a wide range of hydrophobic interactions within the NTD region. The acylamino linker could form hydrogen bond interactions with Asn57 and Gln63. The nitrogen atom on the indole ring could form a hydrogen bond interaction with Gln63, and the indole ring could interact with Met66, Gln67, Lys70, Gln63 of the NTD, and Arg173 and Lys182 of the adjacent CTD [19,25,26]. Previous studies identified numerous novel **PF-74** derivatives with improved potency and metabolic stability [21,25,27–30]. Although they exhibited moderate anti-HIV activity ($EC_{50} = 2.1\text{--}4.3\ \mu\text{M}$), they provided a basis for further modification of **PF-74** (Figure 1b). Our structure–activity relationship studies identified the phenylalanine core region of **PF-74** being crucial for maintaining antiviral activity. The indole group and linker portion acted on the solvent-exposed region with potential for synthetic modifications. Consequently, the linker portion of **PF-74** greatly influences anti-HIV activity.

A “Fraction of sp^3 carbon atoms” (F_{sp^3} , the number of sp^3 hybridized carbons/total carbon count) has been proposed to measure the carbon saturation of molecules and to characterize the complexity of molecular space structures [31–34]. Researchers proposed and successfully proved that the increase in the saturation measured by F_{sp^3} within molecules improved the clinical success rate, which may be related to the increase in solubility or to the increased three-dimensional characteristics crucial to occupying the molecule’s binding site [35,36]. The multicomponent reaction refers to a reaction in which three or more reaction raw materials are used to synthesize a final product with each raw material fragment simultaneously. Compared with the traditional synthesis method, it can shorten the reaction process without separating the intermediates and effectively shorten the reaction time, improving the overall synthesis efficiency [37,38]. In addition, it plays an important role in constructing compound libraries. Therefore, using a fragment-based drug design strategy, we innovatively applied the Ugi four-component reaction to synthesize successfully for the first time, to our knowledge, peptidomimetic-based capsid protein binders with a linker rich in sp^3 hybridization.

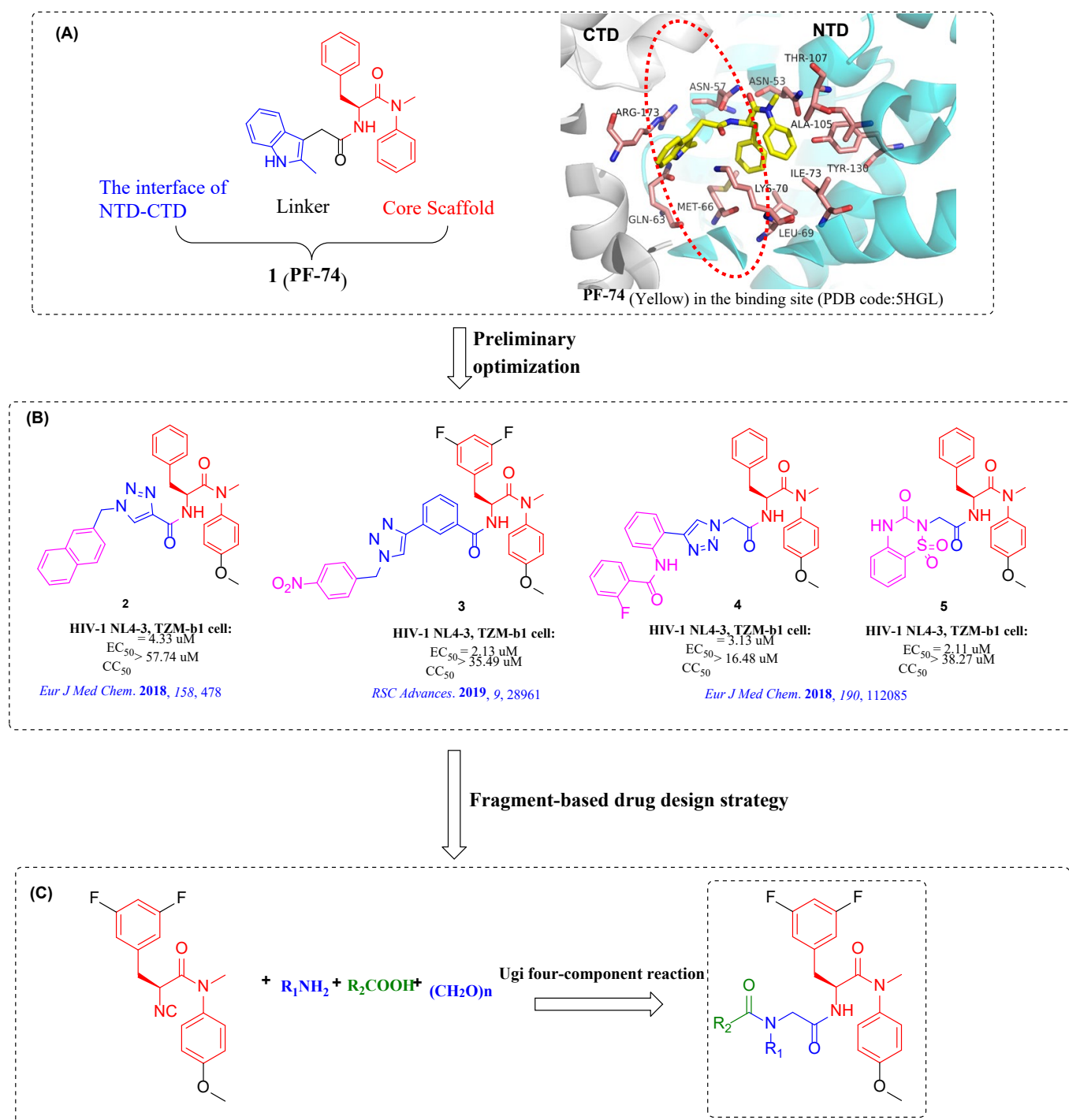


Figure 1. The design of novel phenylalanine derivatives HIV CA modulators (A) Structure and the binding mode of PF-74 within the NTD-CTD interface of an HIV-1 CA hexamer (PDB code: 5HGL). (B) Overview of reported phenylalanine derivatives from our group targeting the HIV-1 CA protein. (C) Schematic route for our Ugi four-component reaction strategy.

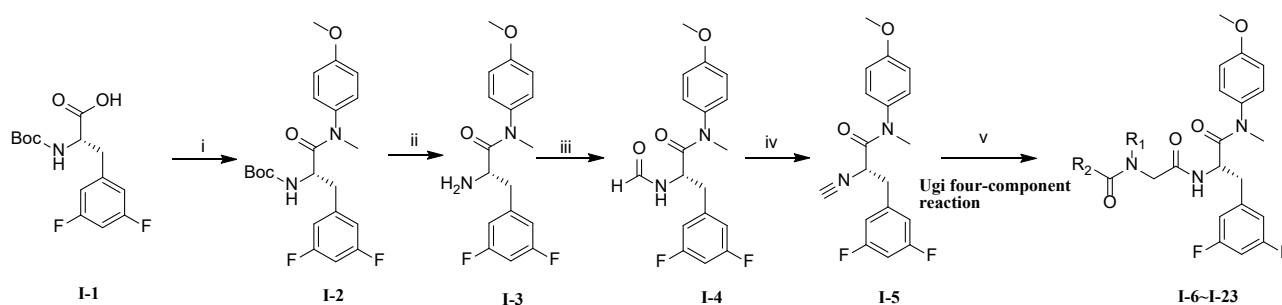
Herein, 18 novel PF-74 derivatives were designed, synthesized, and evaluated for their anti-HIV potency. Furthermore, we demonstrated that the representative compound I-19 interacts with CA using a surface plasmon resonance (SPR) binding assay. In addition, molecular dynamics simulations (MD) were performed on I-19 to explore the binding mode with the CA hexamer. Moreover, we discuss our preliminary structure—activity

relationships (SARs) of PF-74 derivatives, which are essential for further improvement in antivirals targeting the HIV-1 CA protein.

2. Results and Discussion

2.1. Chemistry

As shown in Scheme 1, Boc-*L*-3,5-difluorophenylalanine (**I-1**) amide was treated with *N*-methyl-4-aminoanisole via a condensation reaction to yield intermediate **I-2**. **I-2** was removed from the Boc group under the presence of trifluoroacetic acid to obtain intermediate **I-3**. Next, **I-3** was reacted with ammonium formate to give intermediate **I-4**, which was dehydrated to obtain the key intermediate isocyanide **I-5**. Finally, **I-5** was reacted with various acids, amines, and aldehydes to obtain the target compounds **I-6**–**I-23** via the Ugi four-component reaction [39].



Scheme 1. Reagents and Conditions: (i) 4-methoxy-*N*-methylaniline, HATU, DIEA, CH₂Cl₂, r.t., 8 h; (ii) CF₃COOH, CH₂Cl₂, r.t., 4 h; (iii) ammonium formate, acetonitrile, 90 °C, 24 h; (iv) triethylamine, POCl₃, CH₂Cl₂, 0 °C, 12 h; (v) R₁-NH₂, R₂-COOH, (CH₂O)_n, anhydrous methanol, 60 °C, 8 h.

2.2. Biological Activity

The newly synthesized PF-74 derivatives were tested for anti-HIV activity and cytotoxicity in MT-4 cells using the MTT method. Meanwhile, PF-74 and the approved drug nevirapine (NVP) were selected as controls. The evaluated results of EC₅₀ (anti-HIV-1/2 activity), CC₅₀ (cytotoxicity), and SI (selectivity index, CC₅₀/EC₅₀) are shown in Table 1.

The antiviral activity of this series of compounds against HIV-1 ranged from 30.29 to 2.53 μM. Among them, compound **I-19** (EC₅₀ = 2.53 ± 0.84 μM) had the best antiviral activity against HIV-1, but was still weaker than PF-74 (EC₅₀ = 0.26 ± 0.08 μM). When R₁ was *p*-fluorobenzyl, the activity of different substituents of R₂ on HIV-1 was: 1-methyl-3-(trifluoromethyl)-tetrahydroindazole (**I-19**, EC₅₀ = 2.53 ± 0.84 μM) ≈ 2,3-dimethyl-indole (**I-7**, EC₅₀ = 2.79 ± 0.19 μM) ≈ 3-methyl-5-bromoindole (**I-9**, EC₅₀ = 2.93 ± 0.32 μM) ≈ *p*-methylphenylboronic acid (**I-23**, EC₅₀ = 4.33 ± 1.32 μM) > *p*-methylphenylboronic acid pinacol ester (**I-12**, EC₅₀ = 11.73 ± 2.07 μM). Notably, when R₁ was introduced into a smaller cyclopropyl group, the compounds (**I-11**, EC₅₀ = 3.08 ± 0.15 μM; **I-18**, EC₅₀ = 5.18 ± 1.11 μM) also possessed outstanding activity against HIV-1.

The activity of this series of compounds against HIV-2 ranged from 24.9 to 2.30 μM. Among them, **I-14** (EC₅₀ = 2.30 ± 0.11 μM, CC₅₀ > 189.32 μM) displayed the best anti-HIV-2 activity, which was equivalent to PF-74 (EC₅₀ = 2.22 ± 0.31 μM, CC₅₀ = 73.83 ± 7.54 μM) and better than the approved drug nevirapine (EC₅₀ > 15.02 μM, CC₅₀ > 15.02 μM) and had lower toxicity than both. When R₁ was *p*-cyanobenzyl, the activity of different substituents of R₂ on HIV-2 was: 1-methylnaphthalene (**I-14**, EC₅₀ = 2.30 ± 0.11 μM) > 3-methyl-5-fluoroindole (**I-15**, EC₅₀ = 5.81 ± 1.11 μM) > 3-methyl-5-bromoindole (**I-16**, EC₅₀ = 15.71 ± 13.30 μM) ≈ *p*-methylphenylboronic acid pinacol ester (**I-17**, EC₅₀ = 16.16 ± 4.59 μM).

Table 1. Anti-HIV-1/HIV-2 activity of novel phenylalanine derivatives.

Compound ID	R ₁	R ₂	EC ₅₀ (μM) ^a		CC ₅₀ (μM) ^b	SI ^c	
			HIV-1	HIV-2		HIV-1	HIV-2
I-6			>160.20	>160.20	>160.20	X1 d	X1
I-7			2.79 ± 0.19	>22.59	22.59 ± 0.96	8	X1
I-8			>191.35	5.87 ± 1.79	>191.35	X1	>33
I-9			2.93 ± 0.32	>17.84	17.84 ± 1.04	6	<1
I-10			>17.61	>17.61	17.61 ± 2.41	<1	<1
I-11			3.08 ± 0.15	17.33 ± 3.79	111.60 ± 7.99	36	6
I-12			11.73 ± 2.07	13.21 ± 2.60	65.40 ± 16.77	6	5
I-13			>189.32	161.33 ± 26.04	>189.32	X1	>1
I-14			>189.33	2.30 ± 0.11	>189.32	X1	>82
I-15			17.25 ± 9.98	5.81 ± 1.11	148.30 ± 16.63	9	26
I-16			5.61 ± 1.18	15.71 ± 13.30	87.59 ± 62.25	16	6
I-17			17.65 ± 4.60	16.16 ± 4.59	52.41 ± 14.22	3	3
I-18			5.18 ± 1.11	9.71 ± 0.80	89.05 ± 17.06	17	9

Table 1. Cont.

Compound ID	R ₁	R ₂	EC ₅₀ (μM) ^a		CC ₅₀ (μM) ^b	SI ^c	
			HIV-1	HIV-2		HIV-1	HIV-2
I-19			2.53 ± 0.84	12.93 ± 3.72	107.61 ± 27.43	42	8
I-20			30.29 ± 3.24	24.90 ± 12.04	45.66 ± 5.36	2	2
I-21			2.77 ± 0.77	6.52 ± 0.60	28.63 ± 0.86	10	4
I-22			>176.28	>18.87	176.28 ± 7.35	<1	<1
I-23			4.33 ± 1.32	6.80 ± 0.36	18.91 ± 3.59	4	3
PF-74			0.26 ± 0.08	2.22 ± 0.31	73.83 ± 7.54	297	33
NVP			0.12 ± 0.027	>15.02	>15.02	>123	X1

^a EC₅₀: concentration of compound required to achieve 50% protection of MT-4 cell cultures against HIV-induced cytopathicity, as determined by the MTT method; ^b CC₅₀: the compound concentration required to reduce the viability of uninfected cells by 50%, as determined by the MTT method; ^c SI: selectivity index, the ratio of CC₅₀/EC₅₀; ^d X1: not determined.

When R₁ was *p*-fluorobenzyl and R₂ was indole, the compounds (**I-7**, EC₅₀ (HIV-1) = 2.79 ± 0.19 μM, EC₅₀ (HIV-2) > 22.59 μM; **I-9**, EC₅₀ (HIV-1) = 2.93 ± 0.32 μM, EC₅₀ (HIV-2) > 17.84 μM) had good selectivity to HIV-1. Furthermore, when R₂ was 1-methylnaphthalene, the compounds (**I-15**, EC₅₀ (HIV-1) = 17.25 ± 9.98 μM, EC₅₀ (HIV-2) = 5.81 ± 1.11 μM; **I-14**, EC₅₀ (HIV-1) > 189.33 μM, EC₅₀ (HIV-2) = 2.30 ± 0.11 μM) had marked selectivity to HIV-2. It is worth noting that when the 1-methylnaphthalene of R₂ is replaced by 2-methylnaphthalene, the anti-HIV activity of the compounds (**I-6**, **I-13**) will be lost.

Overall, the study of this series of compounds showed that the change in substituents greatly influenced antiviral activity and selectivity. In this series of compounds, the anti-HIV-2 activity of **I-14** was comparable to **PF-74** and better than the approved drug nevirapine, and the cytotoxicity was lower than that of both, which lays the foundation for the discovery of highly effective anti-HIV inhibitors.

2.3. Surface Plasmon Resonance (SPR) Assay on HIV-1 CA

In order to determine the target of the newly synthesized compounds, compound **I-19** was selected to verify the affinity with HIV-1 CA protein with an SPR experiment. **PF-74** was used as a positive control. As shown in Table 2, Figures 2 and 3, the results indicated that the affinity of the compounds for CA proteins were **PF-74** (hexamer: K_D = 47.0 ± 0.6 nM; monomer: K_D = 968.5 ± 446.7 nM) > **I-19** (hexamer:

$K_D = 36866.7 \pm 12012.6$ nM; monomer: $K_D = 13,338.0 \pm 7793.4$ nM), which is consistent with antiviral activity in vitro (PF-74, $EC_{50} = 0.26 \pm 0.08$ μ M > I-19, $EC_{50} = 2.53 \pm 0.84$ μ M). In contrast to PF-74, I-19 is more inclined to interact with CA monomer. SPR experiments demonstrated that these compounds could be defined as specific HIV-1 CA modulators. The amino acid sequences (GenBank accession number: M30895) and NTD 3-D structure (PDB code: 2WLV) of HIV-2 CA protein are significantly similar to that of HIV-1 (GenBank accession number: AF324493; PDB code: 3H4E). In particular, the amino acids at the binding site of PF-74 are the same, except for amino acids 69 and 70. Therefore, these compounds could also bind to HIV-2 capsid protein.

Table 2. SPR results of I-19 and PF-74 binding to CA monomer and hexamer.

Compound ID	K_D (nM) ^a		K_{on} ($M^{-1}S^{-1}$)		K_{off} (S^{-1})		Ratio ^b
	Monomer	Hexamer	Monomer	Hexamer	Monomer	Hexamer	
I-19	13,338.0 \pm 7793.4	36,866.7 \pm 12012.6	4160 \pm 1670	628 \pm 152	0.0301 \pm 0.0172	0.00758 \pm 0.000504	0.36
PF-74	968.5 \pm 446.7	47.0 \pm 0.6	1,770,000 \pm 1,460,000	756,000 \pm 45,500	1.58 \pm 0.628	0.0363 \pm 0.00692	21

^a All values represent the average response from at least 3 replicates; ^b Ratio: $K_{D(monomer)}/K_{D(hexamer)}$.

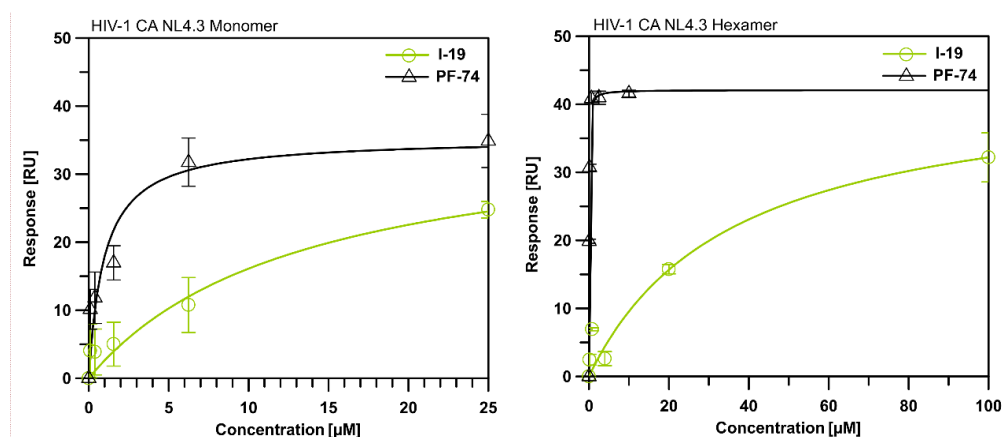


Figure 2. SPR isotherms derived from the equilibrium stage of compounds I-19 and PF-74. All values represent the average response from at least 3 replicates with standard deviations.

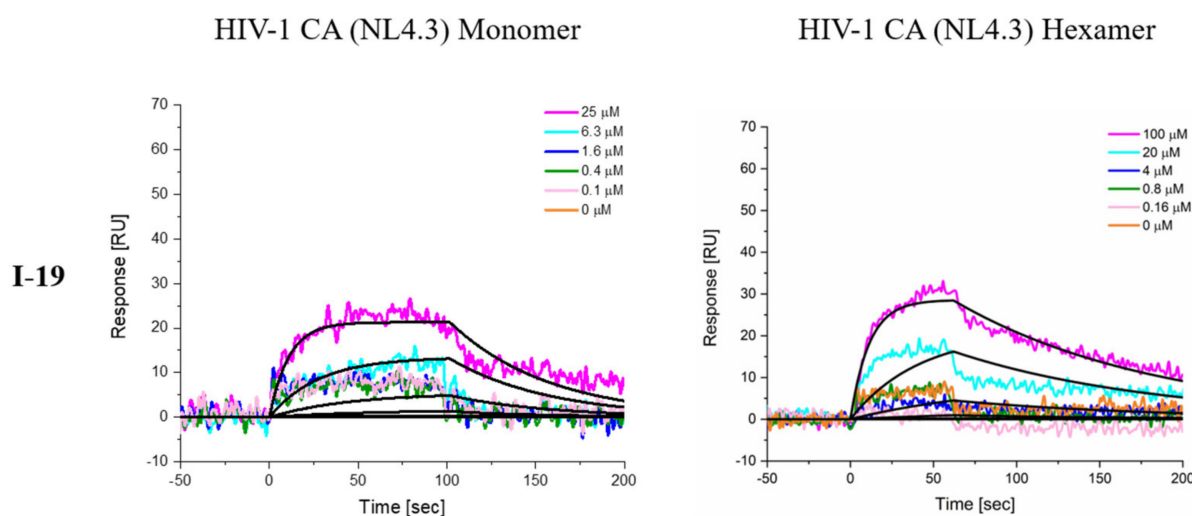


Figure 3. Cont.

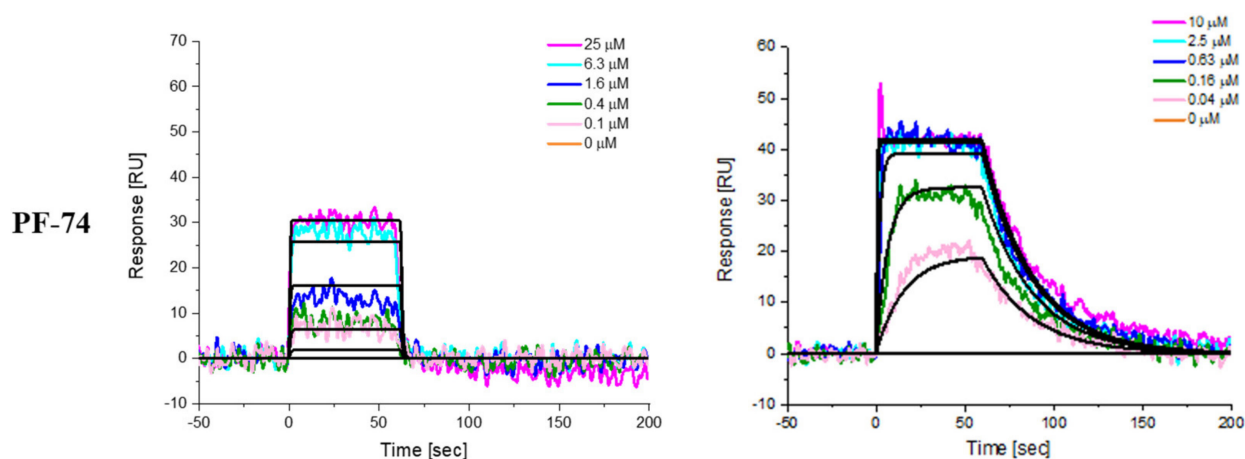


Figure 3. Representative sensorgrams depicting the interaction of **I-19** and **PF-74** with the HIV-1 CA monomer and hexamer. SPR sensorgrams showing (Left Panel) **I-19** and **PF-74** (25 μM starting concentration with 1:4 serial dilutions) binding to immobilized NL4-3 CA monomer, (Right Panel) **I-19** and **PF-74** (100 μM starting concentration with 1:5 serial dilutions for **I-19** and 10 μM starting concentration with 1:4 serial dilutions for **PF-74**) binding to immobilized disulfide-stabilized NL4-3 CA hexamer. Colored lines represent actual data collected from the dilution series, whereas black lines signify the fits to a 1:1 binding model.

2.4. Molecular Docking and MD Simulation

In order to explore the binding mode of these compounds with HIV-1 CA hexamer (PDB codes: 5TSX, 5HGL, <https://www.rcsb.org>), the representative compound **I-19** was selected for molecular docking; the MD simulation and the results were compared with **PF-74**. Compound **I-19** exhibited a docking score, XP gscore, and binding free energy of -4.884 kcal/mol, -4.884 kcal/mol, and -37.23 kcal/mol, respectively. However, **PF-74** showed a docking score, XP gscore, and binding free energy of -5.068 kcal/mol, -5.068 kcal/mol, and -57.72 kcal/mol, respectively. Compound **I-19** showed slightly lower docking results in comparison to **PF-74**, which were in agreement with the experimental values where EC_{50} of **I-19** and **PF-74** was 2.53 ± 0.84 μM and 0.26 ± 0.08 μM , respectively. From the binding modes of **I-19** and **PF-74** with HIV-1 CA, the amide group of the phenylalanine backbone can form a hydrogen bond interaction with Asn57. The nitrogen atom on the indole substituent can form a hydrogen-bonding interaction with Gln63, while the nitrogen atom on the substituent group **I-19** can form a hydrogen-bonding interaction with Gln67 (Figure 4).

Figure 5 and 6 describe the stability of compounds **I-19** and **PF-74** in the binding pocket of HIV-1 CA (PDB code: 5TSX), respectively. In the **I-19**-5TSX complex, the protein structure became stable in the first few ns, and the average root mean square deviation (RMSD) of $\text{C}\alpha$ was 3.8 \AA (Figure 5a). For **I-19**, the structure of the capsid protein was stable at 35 ns, and the RMSD was 0.69 \AA (Figure 5a). The root mean square fluctuation (RMSF) plot shows partial fluctuations in 4-fluorophenyl and indazole (Figure 5b). Compound **I-19** interacts with binding site residues through H bond (green), hydrophobic interaction (grey), and water bridge (blue). **I-19** forms an H bond with Asn57 and Lys70, hydrophobic interaction with Leu56, Lys70, and Ile73, and interaction with Asn53, Leu56, Asn57, and Lys70 through a water bridge (Figure 5c,d). Compound **I-19** maintained 6–7 binding forces with the binding site throughout the molecular dynamics simulation (Figure 5e).

In the **PF-74**-5TSX complex, the protein structure became stable at 40 ns with a RMSD of $C\alpha$ of 5.7 Å. For **PF-74**, the structure of the capsid protein was stabilized at 42 ns with an RMSD of 3.4 ± 0.6 Å (Figure 6a). The RMSF plot of **PF-74** indicated that the indole moiety fluctuated the most during the simulation (Figure 6b). Compounds **I-19** and **PF-74** had similar binding when bound to proteins, but compound **PF-74** had a lower RMSD and RMSF than **I-19**. This indicates that compound **PF-74** has higher affinity and stability than **I-19**. Among them, **PF-74** can form hydrogen-bonding interactions with residues Asn53, Asn57, and Lys70 and can form hydrophobic interactions with residues Leu56, Met66, Lys70, and Ile73 (Figure 6c). The salt bridge interaction did not affect the stability of neither **I-19** nor **PF-74** molecules (Figure 6c). During the entire molecular dynamics simulation, **PF-74** maintained 6–7 binding forces with the binding site (Figure 6d).

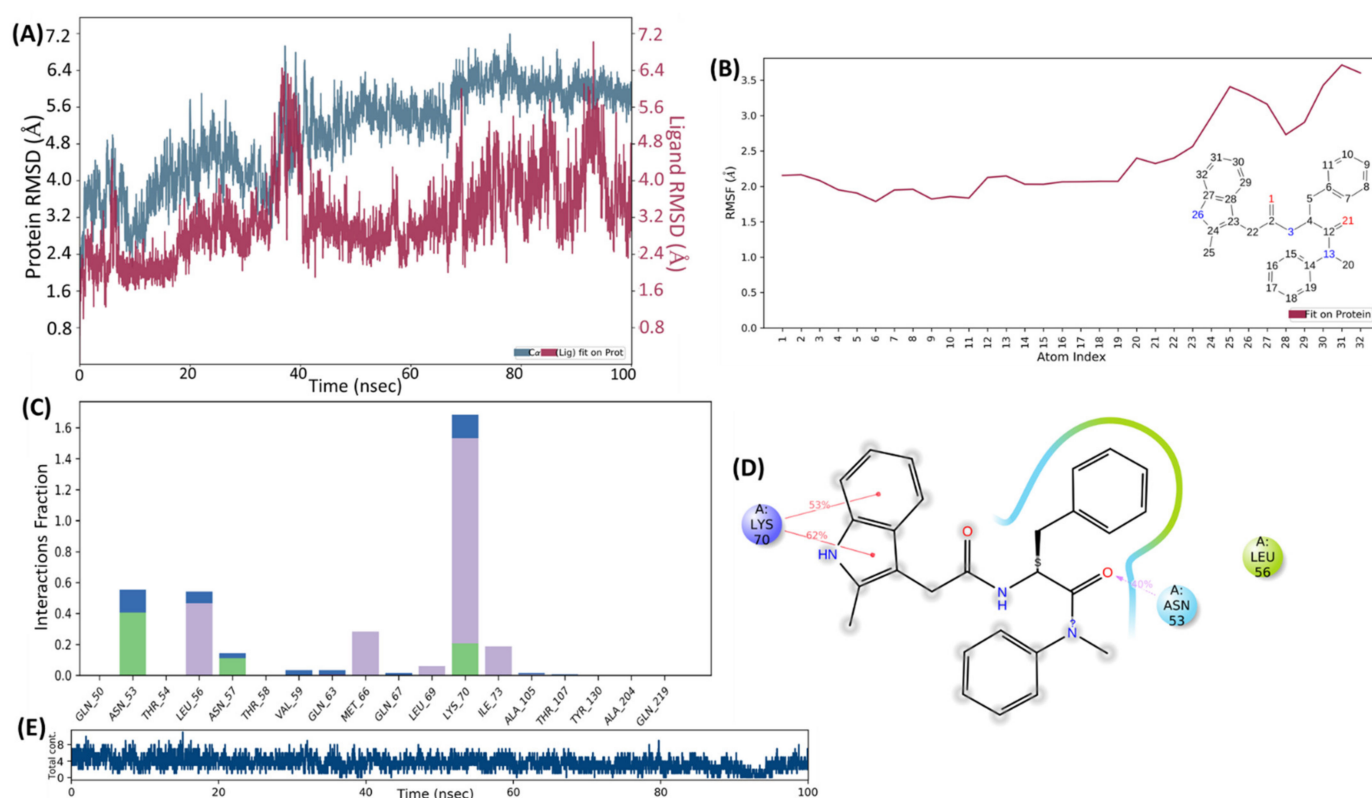


Figure 6. Molecular dynamics simulation process of **PF-74** complex with capsid protein. (A) RMSD plot for $C\alpha$ of capsid protein (PDB code: 5TSX) in complex with **PF-74**; (B) RMSF plots of compound in the CA-**PF-74** complex; (C) The ratio of amino acid residues to the role of **PF-74**; (D) The percentage of interactions in molecular dynamic simulations of **PF-74** complex with capsid; (E) A timeline representation of the interactions and total contacts (H bonds, hydrophobic interactions, and water bridges) obtained during the molecular dynamics simulations. The panels show the total number of specific contacts the capsid made with the **PF-74** throughout the simulation.

The thermal-binding free energy of both the complexes was calculated (after ligand stability) for every 2 ns during simulation by MMGBSA. Compound **I-19** (−53.81 kcal/mol) showed better average binding energy compared to **PF-74** (−44.45 kcal/mol) (Table 3). The H bond and water bridge formation (Figure 5c) during the simulation could play a role in compound **I-19**'s stability, which may be the reason for the better thermal-binding free energy of **I-19** over the **PF-74** during the simulation.

Table 3. Thermal-binding energy calculated (after ligand stability) for every 2 ns during trajectory.

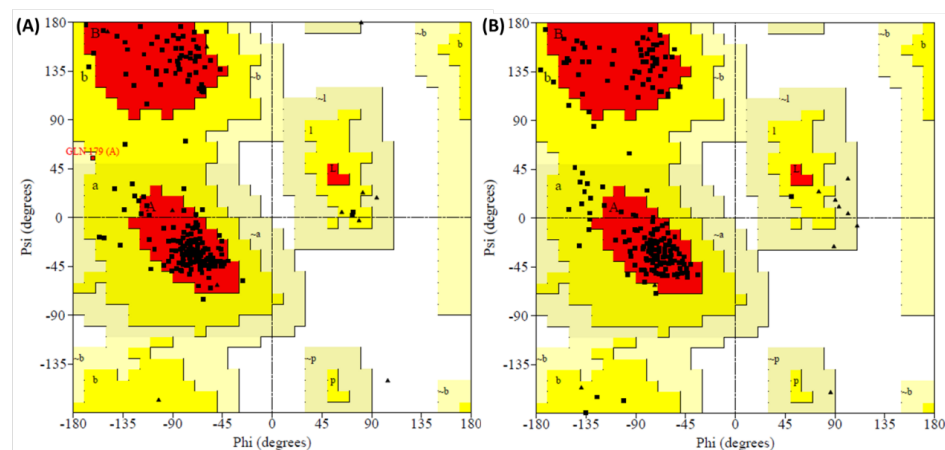
I-19	PF-74	I-19	PF-74
-56.63870297	-48.4265	-47.64271626	-42.9916
-58.18585033	-47.3288	-59.70576824	-42.4198
-44.63984043	-50.9128	-53.24015651	-38.9422
-51.85506041	-48.0358	-50.34292794	-39.1304
-69.09500139	-50.5226	-48.40161062	-40.9924
-52.42678458	-42.4339	-48.80203871	-40.818
-37.40863362	-48.288	-51.18628072	-45.1481
-56.59643919	-43.116	-57.96423626	
-58.20409472	-48.9477	-51.31042621	
-61.13273155	-44.6422	-55.20319794	
-56.26117453	-50.9619	-47.39770192	
-42.66745202	-47.8149	-46.58669711	
-39.143513	-49.8492	-67.89125429	
-52.88091489	-40.7626	-58.99503816	
-57.51528574	-39.4291	-45.4356079	
-48.50930805	-43.8134	-59.82486366	
-46.0713223	-45.8949	-57.89411038	
-61.01377527	-45.0506	-58.09693178	
-59.25622436	-44.6718	-60.99124817	
-52.76749689	-41.9282	-66.82186876	
-56.22260111	-36.215	-50.50954655	
-44.7446381	-43.4079	-52.43726697	
-58.74678608	-40.6441	-56.73687394	

Based on the molecular dynamics simulation, the conformations of CA-I-19 and CA-PF-74 complexes were verified utilizing a Ramachandran plot. No residues were present in the outlier region of the CA-PF-74 and CA-I-19 complex (Table 4).

Table 4. Occurrence of residues in favored, additional allowed, generously allowed, and disallowed regions.

Complex	Residues in Favored Region	Residues in Additional Allowed Region	Residues in Generously Allowed Region	Residues in Disallowed Region
I-19-5TSX	89.3% (167)	10.2% (19)	0.5% (1)	0.0% (0)
PF-74-5TSX	85.6% (160)	14.4% (27)	0.0% (0)	0.0% (0)

In summary, MD studies further explored the binding mode of compounds I-19 and PF-74 with the HIV-1 CA hexamer (Figure 7). Importantly, these results are consistent with direct binding as judged by SPR and antiviral activity, evaluating our workflow and providing important guidance for further structural optimization efforts.

**Figure 7.** Ramachandran plot (A) I-19-capsid complex; (B) PF-74-capsid complex.

3. Conclusions

In this article, taking **PF-74** as the lead compound, 18 novel phenylalanine-containing peptidomimetics were designed and synthesized utilizing the Ugi four-component reaction. The results of antiviral activity in vitro showed that most compounds had single-digit micromolar antiviral activity against HIV-1. Four compounds, **I-7**, **I-9**, **I-19**, and **I-21**, displayed outstanding potency against HIV-1, with the EC₅₀ values ranging from 2.93 μM to 2.53 μM, but there was still a certain gap compared with **PF-74**. The anti-HIV-2 activity of **I-14** (EC₅₀ = 2.30 ± 0.11 μM, CC₅₀ > 189.32 μM) was similar to that of **PF-74** (EC₅₀ > 2.22 ± 0.31 μM, CC₅₀ = 73.83 ± 7.54 μM), and it was better than that of the marketed drug nevirapine (EC₅₀ > 15.02 μM, CC₅₀ > 15.02 μM); at the same time, it had lower toxicity than both, which deserves further research. Notably, when the hydrophobic naphthalene ring was introduced, the compounds had good selectivity for HIV-1/HIV-2. In addition, SPR-binding assays demonstrated that these compounds could be defined as HIV-1 CA modulators. The molecular dynamics simulation analysis indicated the potential binding mode between compound **I-19** and the NTD-CTD interface of the CA hexamer provided important guidance for further structural optimization. In summary, using a fragment-based drug design strategy, the Ugi four-component reaction was applied to the small molecule targeting the HIV capsid protein for the first time, which laid the foundation for the discovery of candidate drugs with excellent antiviral activity and optimized drug-like properties.

4. Materials and Methods

4.1. Chemistry

¹H NMR and ¹³C NMR spectra were recorded on a Bruker Avance-400 NMR spectrometer (Standard G1313A instrument) with DMSO-*d*₆ as the solvent. Chemical shifts were expressed in δ values (ppm) using tetramethylsilane (TMS) as an internal reference, and *J* values were expressed in hertz (Hz). Melting points of all the compounds were determined on a micromelting point apparatus and were uncorrected. Flash column chromatography was performed on a column packed with Silica Gel60 (200–300 mesh). Most of the solvents were obtained from Sinopharm Chemical Reagent Co, Ltd. (SCRC) and were AR grade. TLC was performed on silica Gel GF254 (Merck) and irradiated by ultraviolet light (λ = 254 nm). Flash column chromatography was performed on a column packed with Silica Gel60 (200–300 mesh).

4.1.1. Tert-butyl (S)-(3-(3,5-difluorophenyl)-1-((4-methoxyphenyl)(methyl)amino)-1-oxopropan-2-yl) carbamate (**I-2**)

The starting material Boc-3,5-difluoro-*L*-phenylalanine (mg, 6.64 mmol) and 4-methoxy-*N*-methylaniline (mg, 6.64 mmol) were added to 20 mL dichloromethane and stirred in an ice bath for 30 min. Then, DIEA (2.23 mL, 13.29 mmol) and *N*-methyl-4-aminoanisole (610 mg, 4.43 mmol) were added and stirred at room temperature for another 8 h (monitored by TLC). The mixture was evaporated under reduced pressure, and the residue was washed with saturated sodium bicarbonate (50 mL) and extracted with ethyl acetate (3 × 10 mL). Then, the combined organic layer was washed with 1 N HCl, extracted with ethyl acetate (3 × 10 mL), dried with anhydrous Na₂SO₄, filtered, and concentrated under reduced pressure to afford corresponding crude intermediate **I-2** as a yellow oil with a yield of 60%. ¹H NMR (400 MHz, DMSO-*d*₆) δ 7.31 (d, *J* = 8.6 Hz, 2H, PhH), 7.05 (tt, *J* = 19.0, 9.0 Hz, 4H, PhH), 6.43 (d, *J* = 7.0 Hz, 2H, PhH), 4.14 (td, *J* = 10.6, 3.1 Hz, 1H, CH), 3.80 (s, 3H, OCH₃), 3.15 (d, *J* = 7.8 Hz, 3H, NCH₃), 2.87–2.73 (m, 1H, CH), 2.69–2.57 (m, 1H, CH), 1.29 (s, 9H, 3(CH₃)). ESI-MS: *m/z* 443.78 [M + Na]⁺, C₂₂H₂₆F₂N₂O₄ [420.4].

4.1.2. (S)-2-amino-3-(3,5-difluorophenyl)-*N*-(4-methoxyphenyl)-*N*-methylpropanamide (**I-3**)

Intermediate **I-2** (500 mg, 1.19 mmol) was added to 30 mL dichloromethane, and then trifluoroacetic acid (410 mg, 3.57 mmol) was slowly dropped. The mixture was stirred at room temperature. After 1 h, the reaction was completed. The pH of the reac-

tion solution was adjusted to 7 with saturated sodium bicarbonate solution, and 40 mL dichloromethane was added for extraction. The organic phase was separated, washed with saturated sodium chloride solution (3 × 20 mL), dried with anhydrous Na₂SO₄, filtered, and concentrated under reduced pressure to afford corresponding crude intermediate **I-3** as a yellow oil with a yield of 80%. ¹H NMR (400 MHz, DMSO-*d*₆) δ 7.07 (d, *J* = 8.3 Hz, 2H), 7.05–6.93 (m, 3H), 6.57 (h, *J* = 4.0 Hz, 2H), 3.78 (s, 3H), 3.35 (dd, *J* = 7.6, 5.9 Hz, 1H), 3.09 (s, 3H), 2.74 (dd, *J* = 13.1, 5.8 Hz, 1H), 2.54–2.45 (m, 2H), 1.82 (s, 2H).

4.1.3. (S)-3-(3,5-difluorophenyl)-2-formamido-N-(4-methoxyphenyl)-N-methylpropanamide (**I-4**)

Intermediate **I-3** (340 mg, 1.06 mmol) was added to 10 mL acetonitrile, and then ammonium formate (130 mg, 2.12 mmol) was added to the solution, and heated at 90 °C for 24 h (monitored by TLC). After 24 h, the reaction was completed, filtered, and evaporated under reduced pressure. A total of 20 mL of water was added to the residue and extracted with ethyl acetate (3 × 10 mL). The organic phase was combined and washed with 20 mL saturated sodium chloride solution. The organic phase was dried with anhydrous Na₂SO₄, filtered, and concentrated under reduced pressure. The obtained crude product was separated by silica gel column chromatography to obtain 1.68 g pure yellow oil product of intermediate **I-4** with a yield of 60%. ¹H NMR (400 MHz, DMSO-*d*₆) δ 8.47 (d, *J* = 8.3 Hz, 1H), 7.87 (s, 1H), 7.22 (d, *J* = 8.3 Hz, 2H), 7.05 (td, *J* = 8.9, 4.6 Hz, 4H), 6.50 (h, *J* = 4.3 Hz, 2H), 4.52 (td, *J* = 8.8, 4.5 Hz, 1H), 3.80 (s, 3H), 3.13 (s, 3H), 2.88 (dd, *J* = 13.6, 4.6 Hz, 1H), 2.67 (dd, *J* = 13.7, 9.4 Hz, 1H). ESI-MS: *m/z* 349.3 [M + 1]⁺, C₁₈H₁₈F₂N₂O₃ [348.35]

4.1.4. (S)-3-(3,5-difluorophenyl)-N-(4-methoxyphenyl)-N-methyl-2-(methylidyne-l4-azaneyl)propanamide (**I-5**)

The intermediate **I-4** (410 mg, 1.18 mmol) was added to 10 mL dichloromethane; then, triethylamine (360 mg, 3.54 mmol) was added to the solution, and phosphorus oxychloride (180 mg, 1.18 mmol) was slowly added under ice bath conditions, stirring at 0 °C for 24 h (monitored by TLC). After 24 h, the reaction was completed, quenched by ice water, extracted with dichloromethane (3 × 15 mL), combined with the organic phase, dried with anhydrous sodium sulfate, filtered, concentrated supernatant, mixed with silica gel, and subjected to column chromatography to obtain 170 mg pure product of light-yellow solid **I-5** with a yield of 45%. ¹H NMR (400 MHz, DMSO-*d*₆) δ 7.26–7.10 (m, 3H, PhH), 7.03 (d, *J* = 8.8 Hz, 2H, PhH), 6.76 (hept, *J* = 4.2 Hz, 2H, PhH), 4.48 (dd, *J* = 8.3, 5.8 Hz, 1H, CH), 3.80 (s, 3H, OCH₃), 3.15 (s, 3H, NCH₃), 3.14–3.07 (m, 1H, CH), 2.99 (dd, *J* = 13.6, 8.3 Hz, 1H, CH). ESI-MS: *m/z* 332.2 [M + 1]⁺, C₁₈H₁₇F₂N₂O₂ [331.12].

4.1.5. General Procedure for the Synthesis of Target Compounds **I-(6-23)**

Polyformaldehyde (18 mg, 0.20 mmol) was dissolved in 6.0 mL of anhydrous methanol, and different amines were dissolved in 6.0 mL of anhydrous methanol. Subsequently, different acids were added, stirred at room temperature for 10 min, and then the key intermediate **I-5** was added, heating reflux at 70 °C for 16 h (monitored by TLC). After the reaction was completed, 10 mL saturated sodium bicarbonate solution was added to the residue in the bottle, and 10 mL dichloromethane was used for extraction. The organic phase was separated, 10 mL 1N HCl solution was added for washing, and the organic phase was separated. After washing with 10 mL saturated sodium chloride solution, the organic phase was dried with anhydrous sodium sulfate, filtered, and concentrated under reduced pressure. The crude product was separated using silica gel column chromatography to obtain the target products **I-(6-23)**.

(S)-3-(3,5-difluorophenyl)-2-(2-(N-(4-fluorobenzyl)-2-(naphthalen-2-yl)acetamido)acetamido)-N-(4-methoxyphenyl)-N-methylpropanamide (**I-6**):

Light-yellow solid, yield: 61%, mp: 175–177 °C. ¹H NMR (400 MHz, DMSO-*d*₆) δ 8.56 (d, *J* = 8.2 Hz, 1H), 7.93–7.86 (m, 1H), 7.86–7.80 (m, 2H), 7.69 (d, *J* = 46.7 Hz, 1H), 7.55–7.44 (m, 2H), 7.39–7.32 (m, 1H), 7.30–7.21 (m, 3H), 7.19–7.09 (m, 3H), 7.09–6.96 (m, 3H),

6.60–6.47 (m, 2H), 4.60 (td, $J = 8.8, 7.9, 5.1$ Hz, 1H), 4.53–4.20 (m, 2H), 3.96 (td, $J = 27.6, 27.1, 13.4$ Hz, 3H), 3.84–3.77 (m, 3H), 3.70 (s, 1H), 3.21–3.11 (m, 3H), 2.90 (ddd, $J = 19.1, 14.3, 4.3$ Hz, 1H), 2.75–2.62 (m, 1H). ^{13}C NMR (100 MHz, DMSO- d_6) δ 171.76, 170.90, 169.49 (d, $J = 265.2$ Hz), 162.51 (dd, $J = 245.8, 13.4$ Hz), 159.23, 159.15, 142.54 (t, $J = 9.4$ Hz), 135.84, 134.23 (d, $J = 3.1$ Hz), 133.87, 133.74, 133.46, 133.41, 132.25, 130.26 (d, $J = 8.2$ Hz), 129.48 (d, $J = 8.1$ Hz), 129.19, 128.49, 128.38, 127.98, 127.93, 127.89, 127.81, 126.48, 126.01, 115.84 (d, $J = 21.4$ Hz), 115.54 (d, $J = 21.3$ Hz), 115.33, 115.24, 112.41 (d, $J = 24.4$ Hz), 102.54, 55.94, 55.90, 51.47, 51.33, 49.85, 37.80, 37.34. ESI-MS: m/z 654.70 $[\text{M} + 1]^+$, $\text{C}_{38}\text{H}_{34}\text{F}_3\text{N}_3\text{O}_4$ [653.70].

(S)-3-(3,5-difluorophenyl)-2-(2-(*N*-(4-fluorobenzyl)-2-(2-methyl-1H-indol-3-yl)acetamido)acetamido)-*N*-(4-methoxyphenyl)-*N*-methylpropanamide (**I-7**):

light-yellow solid, yield: 10.20%, mp: 112.5–114.5 °C. ^1H NMR (400 MHz, DMSO- d_6) δ 10.76 (d, $J = 16.8$ Hz, 1H), 8.51 (d, $J = 8.1$ Hz, 1H), 7.34 (d, $J = 8.1$ Hz, 1H), 7.25 (dd, $J = 17.4, 8.2$ Hz, 3H), 7.16 (dd, $J = 8.2, 5.9$ Hz, 2H), 7.07 (dd, $J = 8.7, 5.2$ Hz, 3H), 7.03–6.97 (m, 3H), 6.89 (t, $J = 7.4$ Hz, 1H), 6.50 (dd, $J = 18.1, 6.7$ Hz, 2H), 4.58 (tt, $J = 11.3, 5.5$ Hz, 1H), 4.51–4.40 (m, 1H), 4.18 (d, $J = 15.1$ Hz, 1H), 3.96 (d, $J = 17.6$ Hz, 1H), 3.87 (d, $J = 12.3$ Hz, 1H), 3.81 (s, 3H), 3.72 (d, $J = 17.3$ Hz, 1H), 3.56 (s, 1H), 3.15 (d, $J = 11.0$ Hz, 3H), 2.88 (ddd, $J = 23.4, 13.6, 4.2$ Hz, 1H), 2.74–2.60 (m, 1H), 2.22 (s, 3H). ^{13}C NMR (150 MHz, DMSO- d_6) δ 170.80, 170.21, 167.32, 161.49 (dd, $J = 245.9, 13.1$ Hz), 161.49 (dd, $J = 254.9, 13.1$ Hz), 159.20, 142.39, 135.22, 135.26, 134.26, 130.09 (d, $J = 7.6$ Hz), 129.74, 129.46 (d, $J = 8.2$ Hz), 129.18, 125.96, 125.90, 123.91, 123.82, 121.69, 121.59, 115.77, 115.66, 115.45, 115.38, 115.36, 115.20, 113.70, 113.69, 112.40, 112.42, 112.31, 112.28, 111.42, 108.50, 102.42, 102.28, 55.86, 51.50, 49.94, 49.18, 37.76, 37.31, 30.33, 15.32. ESI-MS: m/z 657.71 $[\text{M} + 1]^+$, $\text{C}_{37}\text{H}_{35}\text{F}_3\text{N}_4\text{O}_4$ [656.71].

(S)-3-(3,5-difluorophenyl)-2-(2-(*N*-(4-fluorobenzyl)-2-(naphthalen-1-yl)acetamido)acetamido)-*N*-(4-methoxyphenyl)-*N*-methylpropanamide (**I-8**):

light-yellow solid, yield: 10.20%, mp: 112.5–114.5 °C. ^1H NMR (400 MHz, DMSO- d_6) δ 8.59 (d, $J = 8.1$ Hz, 1H), 7.92–7.79 (m, 3H), 7.52–7.41 (m, 3H), 7.26 (ddd, $J = 14.5, 12.3, 7.2$ Hz, 5H), 7.18–7.12 (m, 2H), 7.06 (d, $J = 8.6$ Hz, 2H), 6.94–6.83 (m, 1H), 6.53 (dt, $J = 10.2, 5.0$ Hz, 2H), 4.71–4.56 (m, 1H), 4.51 (t, $J = 14.4$ Hz, 1H), 4.21–4.11 (m, 2H), 4.05–3.93 (m, 3H), 3.80 (d, $J = 7.6$ Hz, 3H), 3.13 (s, 3H), 2.96–2.84 (m, 1H), 2.74–2.64 (m, 1H). ^{13}C NMR (100 MHz, DMSO- d_6) δ 171.75, 170.87, 168.54, 163.70 (d, $J = 13.1$ Hz), 163.06, 161.32, 159.23, 142.49, 135.87, 134.35, 133.75, 133.10 (d, $J = 43.3$ Hz), 130.25 (d, $J = 8.1$ Hz), 129.57 (d, $J = 8.2$ Hz), 129.21, 128.43 (d, $J = 40.3$ Hz), 127.59, 127.50, 126.36, 126.17, 126.04, 125.94, 125.89, 125.77, 125.09, 115.91 (d, $J = 21.5$ Hz), 115.54 (d, $J = 21.2$ Hz), 115.31, 112.49 (d, $J = 6.4$ Hz), 112.31 (d, $J = 6.5$ Hz), 102.49 (t, $J = 25.7$ Hz), 55.91, 51.67, 49.92, 49.27, 37.83, 37.45, 37.28. ESI-MS: m/z 654.5 $[\text{M} + 1]^+$, $\text{C}_{38}\text{H}_{34}\text{F}_3\text{N}_3\text{O}_4$ [653.70].

(S)-2-(2-(2-(5-bromo-1H-indol-3-yl)-*N*-(4-fluorobenzyl)acetamido)acetamido)-3-(3,5-difluorophenyl)-*N*-(4-methoxyphenyl)-*N*-methylpropanamide (**I-9**):

White solid, yield 9.60%, mp: 78–80 °C. ^1H NMR (400 MHz, DMSO- d_6) δ 11.11 (d, $J = 2.4$ Hz, 1H), 8.57 (t, $J = 8.3$ Hz, 1H), 7.73–7.66 (m, 1H), 7.31 (dd, $J = 13.5, 8.5$ Hz, 4H), 7.23–7.17 (m, 4H), 7.11–7.06 (m, 3H), 6.56–6.47 (m, 3H), 5.47 (dd, $J = 10.3, 7.2$ Hz, 1H), 4.63–4.48 (m, 2H), 4.19 (dd, $J = 15.0, 6.6$ Hz, 1H), 4.05–3.91 (m, 2H), 3.80 (d, $J = 1.5$ Hz, 3H), 3.63 (d, $J = 9.5$ Hz, 2H), 3.15 (d, $J = 9.5$ Hz, 3H), 2.90 (td, $J = 14.0, 6.6$ Hz, 1H), 2.71 (dd, $J = 13.5, 9.5$ Hz, 1H). ^{13}C NMR (150 MHz, DMSO- d_6) δ 171.90, 170.86, 168.41, 162.54 (dd, $J = 246.1, 13.2$ Hz), 162.54 (dd, $J = 246.1, 13.2$ Hz), 159.23, 142.50, 135.86, 135.34, 134.32, 130.18 (d, $J = 7.7$ Hz), 129.75, 129.41 (d, $J = 8.3$ Hz), 129.16, 125.99, 125.91, 123.92, 123.86, 121.79, 121.64, 115.83, 115.69, 115.50, 115.36, 115.31, 115.26, 113.74, 113.71, 112.46, 112.43, 112.33, 112.30, 111.50, 108.51, 102.47, 102.30, 55.91, 51.55, 49.92, 49.15, 37.79, 37.34, 30.37. ESI-MS: m/z 757.26 $[\text{M} + 2\text{Na}]^+$, $\text{C}_{36}\text{H}_{32}\text{BrF}_3\text{N}_4\text{O}_4$ [721.58].

(S)-2-(2-(2-(5-bromo-1H-indol-3-yl)-N-(cyclohexylmethyl)acetamido)acetamido)-3-(3,5-difluorophenyl)-N-(4-methoxyphenyl)-N-methylpropanamide (**I-10**):

White solid, yield 9.80%, mp: 80–82 °C. ¹H NMR (400 MHz, DMSO-*d*₆) δ 11.08 (d, *J* = 6.4 Hz, 1H), 8.51 (t, *J* = 9.1 Hz, 1H), 7.74–7.65 (m, 1H), 7.31 (dd, *J* = 8.5, 4.0 Hz, 2H), 7.26–7.13 (m, 2H), 7.11–6.90 (m, 3H), 6.52 (d, *J* = 7.0 Hz, 2H), 4.66–4.43 (m, 1H), 4.06–3.86 (m, 2H), 3.79 (d, *J* = 3.8 Hz, 3H), 3.77–3.67 (m, 1H), 3.54 (dd, *J* = 17.0, 7.8 Hz, 1H), 3.14 (d, *J* = 9.6 Hz, 3H), 3.12–3.03 (m, 1H), 2.95 (dd, *J* = 17.0, 5.3 Hz, 1H), 2.88 (dd, *J* = 17.0, 3.7 Hz, 1H), 2.75 (ddd, *J* = 26.8, 13.3, 8.3 Hz, 1H), 1.59–1.56 (m, 1H), 1.52–0.69 (m, 10H). ¹³C NMR (100 MHz, DMSO-*d*₆) δ 171.70, 170.91, 168.75, 168.31, 162.50 (d, *J* = 232.9 Hz), 159.22, 135.86, 135.30 (d, *J* = 4.8 Hz), 129.67 (d, *J* = 2.3 Hz), 129.21, 125.82, 123.79, 121.85, 115.31, 112.56 (dd, *J* = 226.7, 7.3 Hz), 112.49, 112.25, 108.77, 102.48, 55.92, 52.81, 51.50, 51.02, 37.79, 37.24, 36.96, 36.04, 30.71, 30.48, 30.35, 26.52, 25.79. ESI-MS: *m/z* 726.6 [M + NH₄⁺]⁺, C₃₆H₃₉BrF₂N₄O₄ [709.63].

(S)-2-(2-(N-cyclopropyl-2-(2-methyl-1H-indol-3-yl)acetamido)acetamido)-N-(4-methoxyphenyl)-N-methyl-3-phenylpropanamide (**I-11**):

White solid, yield 9.80%, mp: 98–100 °C. ¹H NMR (400 MHz, DMSO-*d*₆) δ 10.71 (s, 1H), 8.16 (d, *J* = 8.2 Hz, 1H), 7.34 (d, *J* = 7.8 Hz, 1H), 7.19 (dd, *J* = 8.2, 2.8 Hz, 3H), 6.99 (t, *J* = 8.1 Hz, 3H), 6.93 (t, *J* = 7.4 Hz, 1H), 6.85 (t, *J* = 7.2 Hz, 1H), 6.47 (d, *J* = 6.7 Hz, 2H), 4.45 (td, *J* = 8.8, 4.6 Hz, 1H), 3.94 (d, *J* = 16.5 Hz, 1H), 3.85 (d, *J* = 17.0 Hz, 2H), 3.76 (d, *J* = 5.4 Hz, 3H), 3.71 (s, 1H), 3.10 (d, *J* = 9.2 Hz, 3H), 2.83 (dd, *J* = 13.5, 4.1 Hz, 1H), 2.69–2.57 (m, 1H), 2.26 (s, 3H), 2.22–2.10 (m, 1H), 1.33–1.11 (m, 2H), 0.71–0.64 (m, 2H). ¹³C NMR (150 MHz, DMSO-*d*₆) δ 171.82, 170.82, 168.36, 162.50 (dd, *J* = 246.1, 13.2 Hz), 159.21, 142.46, 135.81, 135.30, 130.16 (d, *J* = 7.7 Hz), 129.39 (d, *J* = 8.3 Hz), 125.96, 125.86, 123.91, 123.79, 121.76, 121.62, 115.82, 115.66, 115.48, 115.32, 113.70, 113.69, 112.45, 112.41, 112.30, 112.28, 111.49, 108.46, 102.45, 102.28, 55.90, 49.86, 49.12, 37.70, 37.30, 32.11, 30.32, 4.82, 4.82. ESI-MS: *m/z* 589.31 [M + 1]⁺, C₃₃H₃₄F₂N₄O₄ [588.66].

(S)-3-(3,5-difluorophenyl)-2-(2-(N-(4-fluorobenzyl)-2-(4-(4,4,5,5-tetramethyl-1,3,2-dioxaborolan-2-yl)phenyl)acetamido)acetamido)-N-(4-methoxyphenyl)-N-methylpropanamide (**I-12**):

White solid, yield 10.5%, mp: 98–100 °C. ¹H NMR (400 MHz, DMSO-*d*₆) δ 8.51 (d, *J* = 8.3 Hz, 1H), 7.59 (t, *J* = 6.8 Hz, 2H), 7.27–7.24 (m, 2H), 7.22–7.19 (m, 2H), 7.15 (dd, *J* = 10.9, 7.8 Hz, 4H), 7.06–7.00 (m, 3H), 6.50 (t, *J* = 6.7 Hz, 2H), 4.56 (ddd, *J* = 17.0, 10.9, 6.0 Hz, 1H), 4.42 (dd, *J* = 14.5, 7.6 Hz, 1H), 4.18 (d, *J* = 15.0 Hz, 1H), 3.96–3.88 (m, 2H), 3.82 (d, *J* = 8.3 Hz, 3H), 3.54 (s, 2H), 3.14 (d, *J* = 12.0 Hz, 3H), 2.94–2.81 (m, 1H), 2.73–2.61 (m, 1H), 1.29 (s, 12H). ¹³C NMR (150 MHz, DMSO-*d*₆) δ 171.50, 170.80, 168.07, 162.68, 161.77, 161.68, 161.07, 159.24, 142.51, 142.45, 139.55, 139.44, 135.84, 134.88, 134.82, 134.77, 134.16 (d, *J* = 3.0 Hz), 130.24 (d, *J* = 8.1 Hz), 129.44 (d, *J* = 8.2 Hz), 129.33, 129.31, 129.24, 129.12, 115.86, 115.72, 115.50 (d, *J* = 21.3 Hz), 115.31, 115.25, 112.39 (d, *J* = 24.6 Hz), 102.45, 102.28, 84.00, 83.98, 55.89, 51.43, 49.79, 49.06, 47.69, 41.48, 37.76, 37.44, 25.38, 25.08. ESI-MS: *m/z* 730.16 [M + 1]⁺, 752.50 [M + Na]⁺, C₄₀H₄₃BF₃N₃O₆ [729.60].

(S)-2-(2-(N-(4-cyanobenzyl)-2-(naphthalen-2-yl)acetamido)acetamido)-3-(3,5-difluorophenyl)-N-(4-methoxyphenyl)-N-methylpropanamide (**I-13**):

White solid, yield 7.80%, mp: 60–62 °C. ¹H NMR (400 MHz, DMSO-*d*₆) δ 8.60 (d, *J* = 8.3 Hz, 1H), 7.86 (dt, *J* = 14.0, 6.9 Hz, 3H), 7.76 (t, *J* = 6.8 Hz, 2H), 7.67 (d, *J* = 22.8 Hz, 1H), 7.49 (p, *J* = 6.2, 5.6 Hz, 2H), 7.44–7.18 (m, 5H), 7.13–6.91 (m, 3H), 6.67–6.41 (m, 2H), 4.79–4.48 (m, 2H), 4.39 (d, *J* = 16.0 Hz, 1H), 4.20–3.95 (m, 2H), 3.82 (d, *J* = 19.2 Hz, 3H), 3.70 (dd, *J* = 16.1, 6.3 Hz, 2H), 3.15 (d, *J* = 14.7 Hz, 3H), 2.90 (td, *J* = 15.1, 14.5, 6.6 Hz, 1H), 2.70 (dd, *J* = 13.6, 10.0 Hz, 1H). ¹³C NMR (150 MHz, DMSO-*d*₆) δ 172.08, 170.80, 168.16, 162.52 (dd, *J* = 246.0, 13.3 Hz), 159.25, 144.11, 142.49, 135.84, 133.75, 133.43, 132.86, 132.66, 132.30, 129.15, 128.88, 128.49, 128.27, 128.14, 128.07, 127.99, 127.97, 127.93, 127.90, 127.82, 126.48, 126.42, 126.02, 119.27, 115.34, 115.25, 112.40 (d, *J* = 24.9 Hz), 110.30, 102.50, 102.32,

55.94, 52.12, 51.49, 50.56, 50.17, 37.80, 37.41. ESI-MS: m/z 661.12 $[M + 1]^+$, 683.52 $[M + Na]^+$. $C_{39}H_{34}F_2N_4O_4$ [660.72].

(S)-2-(2-(N-(4-cyanobenzyl)-2-(naphthalen-1-yl)acetamido)acetamido)-3-(3,5-difluorophenyl)-N-(4-methoxyphenyl)-N-methylpropanamide (**I-14**):

Light-yellow solid, yield 10.60%, mp: 106–108 °C. 1H NMR (400 MHz, DMSO- d_6) δ 8.63 (d, $J = 8.1$ Hz, 1H), 7.90 (d, $J = 7.4$ Hz, 1H), 7.87–7.76 (m, 4H), 7.53–7.45 (m, 2H), 7.41 (q, $J = 10.3, 8.8$ Hz, 3H), 7.34–7.20 (m, 3H), 7.04 (dd, $J = 16.3, 8.8$ Hz, 2H), 6.86 (d, $J = 9.4$ Hz, 1H), 6.51 (t, $J = 6.4$ Hz, 2H), 4.63–4.46 (m, 2H), 4.39–4.16 (m, 2H), 4.14–3.95 (m, 3H), 3.80 (d, $J = 5.4$ Hz, 3H), 3.12 (s, 3H), 2.89 (td, $J = 14.9, 14.3, 6.7$ Hz, 1H), 2.76–2.62 (m, 1H). ^{13}C NMR (100 MHz, DMSO- d_6) δ 172.85, 171.66, 169.36, 164.42, 162.04 (d, $J = 13.0$ Hz), 160.04, 145.11, 143.25 (t, $J = 9.3$ Hz), 135.61 (d, $J = 212.5$ Hz), 134.01, 133.74 (d, $J = 12.6$ Hz), 133.50, 130.02, 129.65, 129.28 (d, $J = 32.1$ Hz), 128.34, 126.99, 126.66 (d, $J = 18.0$ Hz), 125.90, 120.14, 116.12, 113.20 (d, $J = 24.4$ Hz), 111.03, 56.73, 52.51, 51.40, 51.15, 38.64, 38.17, 38.07. ESI-MS: m/z 683.54 $[M + Na]^+$, $C_{39}H_{34}F_2N_4O_4$ [660.72].

(S)-2-(2-(N-(4-cyanobenzyl)-2-(5-fluoro-2-methyl-1H-indol-3-yl)acetamido)acetamido)-3-(3,5-difluorophenyl)-N-(4-methoxyphenyl)-N-methylpropanamide (**I-15**):

Light-yellow solid, yield 10.50%, mp: 120–122 °C. 1H NMR (400 MHz, DMSO- d_6) δ 10.98 (d, $J = 15.4$ Hz, 1H), 8.57 (d, $J = 8.1$ Hz, 1H), 7.85–7.64 (m, 2H), 7.37–7.31 (m, 2H), 7.29–7.23 (m, 3H), 7.19 (dd, $J = 14.2, 2.3$ Hz, 1H), 7.09–6.96 (m, 3H), 6.91 (tq, $J = 8.6, 2.6$ Hz, 1H), 6.52 (d, $J = 6.0$ Hz, 2H), 4.67–4.45 (m, 2H), 4.42–4.02 (m, 2H), 4.02–3.91 (m, 1H), 3.80 (d, $J = 2.8$ Hz, 3H), 3.75 (s, 1H), 3.61 (s, 1H), 3.14 (d, $J = 8.2$ Hz, 3H), 2.89 (td, $J = 15.5, 14.6, 6.6$ Hz, 1H), 2.69 (ddd, $J = 19.6, 11.9, 4.3$ Hz, 1H). ^{13}C NMR (100 MHz, DMSO- d_6) δ 172.82, 171.51, 169.16, 164.42 (d, $J = 13.0$ Hz), 162.08 (d, $J = 13.3$ Hz), 159.94 (d, $J = 10.1$ Hz), 157.20 (d, $J = 10.4$ Hz), 143.35, 135.61, 136.25 (d, $J = 8.1$ Hz), 133.40, 130.08, 129.56, 126.75, 124.60, 122.48 (d, $J = 21.0$ Hz), 120.22, 116.03, 114.35, 113.08 (d, $J = 24.6$ Hz), 112.27, 110.89, 109.16, 103.31, 56.62, 52.34, 52.01, 51.36, 51.02, 38.58, 30.78. ESI-MS: m/z 668.34 $[M + 1]^+$, $C_{36}H_{32}F_4N_4O_4$ [667.24].

(S)-2-(2-(2-(5-bromo-2-methyl-1H-indol-3-yl)-N-(4-cyanobenzyl)acetamido)acetamido)-3-(3,5-difluorophenyl)-N-(4-methoxyphenyl)-N-methylpropanamide (**I-16**):

Light-yellow solid, yield 11.20%, mp: 120–122 °C. 1H NMR (400 MHz, DMSO- d_6) δ 11.08 (d, $J = 13.8$ Hz, 1H), 8.55 (d, $J = 8.1$ Hz, 1H), 7.73 (dd, $J = 12.1, 8.2$ Hz, 2H), 7.63 (d, $J = 21.8$ Hz, 1H), 7.35–7.16 (m, 6H), 7.09–6.91 (m, 3H), 6.51 (d, $J = 5.9$ Hz, 2H), 4.66–4.43 (m, 2H), 4.34 (d, $J = 15.9$ Hz, 1H), 4.19–3.88 (m, 2H), 3.84–3.73 (m, 4H), 3.62 (s, 1H), 3.14 (d, $J = 10.0$ Hz, 3H), 2.89 (td, $J = 14.9, 14.2, 6.6$ Hz, 1H), 2.67 (ddd, $J = 17.7, 13.6, 9.5$ Hz, 1H). ^{13}C NMR (100 MHz, DMSO- d_6) δ 172.96, 171.65, 169.23, 164.54 (d, $J = 13.4$ Hz), 162.09 (d, $J = 13.3$ Hz), 159.98 (d, $J = 10.2$ Hz), 145.11, 143.27, 136.63, 136.07 (d, $J = 8.0$ Hz), 133.40, 130.00, 129.60, 126.83, 124.67, 122.49 (d, $J = 21.0$ Hz), 120.11, 116.11, 114.53, 113.18 (d, $J = 24.7$ Hz), 112.28, 110.99, 109.20, 103.33, 56.74, 52.40, 52.11, 51.39, 51.04, 38.60, 30.99. ESI-MS: m/z 738.52 $[M + 1]^+$, $C_{37}H_{32}BrF_2N_5O_4$ [737.20].

(S)-2-(2-(N-(4-cyanobenzyl)-2-(4-(4,4,5,5-tetramethyl-1,3,2-dioxaborolan-2-yl)phenyl)acetamido)acetamido)-3-(3,5-difluorophenyl)-N-(4-methoxyphenyl)-N-methylpropanamide (**I-17**):

Light-yellow solid, yield 11.20%, mp: 46–48 °C. 1H NMR (400 MHz, DMSO- d_6) δ 8.24 (d, $J = 8.1$ Hz, 1H), 7.60 (d, $J = 7.6$ Hz, 2H), 7.24 (t, $J = 8.0$ Hz, 4H), 7.02 (d, $J = 8.4$ Hz, 3H), 6.51 (d, $J = 6.8$ Hz, 2H), 4.47 (tt, $J = 10.9, 5.4$ Hz, 1H), 4.01–3.88 (m, 3H), 3.80 (s, 3H), 3.71 (d, $J = 28.8$ Hz, 1H), 3.13 (s, 3H), 2.87 (dd, $J = 13.5, 4.2$ Hz, 1H), 2.70–2.66 (m, 1H), 1.29 (s, 12H), 0.74–0.58 (m, 4H). ^{13}C NMR (100 MHz, DMSO- d_6) δ 170.76, 168.07, 162.49 (dd, $J = 246.0, 13.4$ Hz), 159.21, 144.08, 139.46, 135.79, 134.76, 132.89, 132.70, 129.41, 129.28, 129.16, 128.81, 128.10, 119.30, 115.31, 112.39 (d, $J = 24.6$ Hz), 110.24, 84.02, 74.00, 55.93, 55.91, 51.45, 50.41, 50.06, 37.78, 37.34, 25.42, 25.13. ESI-MS: m/z 759.56 $[M + Na]^+$, $C_{41}H_{43}BF_2N_4O_6$ [736.20].

(S)-2-(2-(N-cyclopropyl-2-(4-(4,4,5,5-tetramethyl-1,3,2-dioxaborolan-2-yl)phenyl)acetamido)acetamido)-3-(3,5-difluorophenyl)-N-(4-methoxyphenyl)-N-methylpropanamide (**I-18**):

Light-yellow solid, yield 11.20%, mp: 46–48 °C. ^1H NMR (400 MHz, DMSO- d_6) δ 8.24 (d, J = 8.1 Hz, 1H), 7.60 (d, J = 7.6 Hz, 2H), 7.24 (t, J = 8.0 Hz, 4H), 7.02 (d, J = 8.4 Hz, 3H), 6.51 (d, J = 6.8 Hz, 2H), 4.47 (tt, J = 10.9, 5.4 Hz, 1H), 4.01–3.88 (m, 3H), 3.80 (s, 3H), 3.71 (d, J = 28.8 Hz, 1H), 3.13 (s, 3H), 2.87 (dd, J = 13.5, 4.2 Hz, 1H), 2.70–2.66 (m, 1H), 1.29 (s, 12H), 0.74–0.58 (m, 4H). ^{13}C NMR (100 MHz, DMSO- d_6) δ 173.20, 170.91, 168.57, 162.50 (dd, J = 245.7, 13.4 Hz), 159.14, 142.56, 139.85, 135.83, 134.70, 129.52, 129.15, 115.28, 112.50, 112.26, 102.43, 84.00, 55.91, 51.22, 49.51, 37.76, 37.39, 31.25, 25.42, 25.13, 9.03, 8.86. ESI-MS: m/z 662.17 [M + 1] $^+$, 684.54 [M + Na] $^+$, C₃₆H₄₂BF₂N₃O₆ [661.31].

(S)-3-(3,5-difluorophenyl)-2-(2-(N-(4-fluorobenzyl)-2-(3-(trifluoromethyl)-4,5,6,7-tetrahydro-1H-indazol-1-yl)acetamido)acetamido)-N-(4-methoxyphenyl)-N-methylpropanamide (**I-19**):

Light-yellow solid, yield 11.20%, mp: 46–48 °C. ^1H NMR (400 MHz, DMSO- d_6) δ 8.61 (d, J = 8.2 Hz, 1H), 7.28–7.21 (m, 4H), 7.15 (t, J = 8.8 Hz, 2H), 7.04 (d, J = 8.9 Hz, 2H), 7.01–6.95 (m, 1H), 6.51 (dd, J = 15.1, 7.4 Hz, 2H), 5.19 (s, 1H), 4.99 (s, 2H), 4.58–4.41 (m, 2H), 4.05 (d, J = 15.8 Hz, 2H), 3.97–3.86 (m, 1H), 3.79 (d, J = 7.0 Hz, 3H), 3.73–3.63 (m, 1H), 3.13 (d, J = 7.6 Hz, 3H), 2.95–2.83 (m, 1H), 2.67 (dd, J = 13.6, 9.6 Hz, 1H), 2.49–2.28 (m, 3H), 1.88–1.50 (m, 5H). ^{13}C NMR (100 MHz, DMSO- d_6) δ 170.70, 167.84, 167.62, 163.79, 161.35, 161.21, 159.21, 142.16, 135.78, 133.58, 130.33, 130.25, 129.82, 129.18, 115.89, 115.71, 115.49, 115.31, 114.50, 112.55, 112.48, 112.30, 102.51, 55.87, 51.61, 51.09, 49.41, 49.02, 37.82, 37.31, 22.41, 21.94, 20.90, 20.00. ESI-MS: m/z 716.28 [M + 1] $^+$, C₃₆H₃₅F₆N₅O₄. [715.26].

(S)-2-(2-(N-(cyclohexylmethyl)-2-(5-methyl-3-(trifluoromethyl)-1H-pyrazol-1-yl)acetamido)acetamido)-3-(3,5-difluorophenyl)-N-(4-methoxyphenyl)-N-methylpropanamide (**I-20**):

light-yellow solid, yield 11.20%, mp: 46–48 °C. ^1H NMR (400 MHz, DMSO- d_6) δ 8.64 (d, J = 8.2 Hz, 1H), 7.26 (dd, J = 27.4, 8.7 Hz, 2H), 7.06–6.95 (m, 3H), 6.51 (dd, J = 17.3, 5.6 Hz, 3H), 5.23–4.92 (m, 2H), 4.61–4.47 (m, 1H), 4.13–3.91 (m, 2H), 3.79 (d, J = 6.2 Hz, 3H), 3.14 (d, J = 10.7 Hz, 5H), 2.91 (td, J = 15.9, 14.8, 6.8 Hz, 1H), 2.71 (dd, J = 13.6, 9.5 Hz, 1H), 2.14 (d, J = 20.2 Hz, 4H), 1.55–0.81 (m, 10H). ^{13}C NMR (100 MHz, DMSO- d_6) δ 170.76, 168.24, 167.24, 162.49 (dd, J = 245.8, 13.4 Hz), 159.22, 142.47, 135.80, 129.21, 129.13, 115.33, 115.25, 112.54, 112.30, 103.91, 102.50, 55.87, 53.12, 51.72, 51.57, 49.95, 37.82, 37.28, 35.98, 30.62, 30.52, 26.47, 25.77, 25.72, 10.90. ESI-MS: m/z 662.36 [M – 1] $^-$, C₃₃H₃₈F₅N₅O₄ [663.28].

(S)-2-(2-(N-benzyl-2-(2-methyl-1H-indol-3-yl)acetamido)acetamido)-3-(3,5-difluorophenyl)-N-(4-methoxyphenyl)-N-methylpropanamide (**I-21**):

Light-yellow solid, yield 11.50%, mp: 86–88 °C. ^1H NMR (400 MHz, DMSO- d_6) δ 10.78 (d, J = 15.8 Hz, 1H), 8.53 (d, J = 8.1 Hz, 1H), 7.38 (d, J = 7.8 Hz, 1H), 7.29 (d, J = 8.7 Hz, 2H), 7.26–7.22 (m, 3H), 7.16–7.09 (m, 2H), 7.07 (d, J = 8.4 Hz, 2H), 7.04–6.97 (m, 3H), 6.94–6.88 (m, 1H), 6.59–6.44 (m, 2H), 4.62 (ddd, J = 16.5, 10.3, 5.7 Hz, 1H), 4.54–4.44 (m, 1H), 4.21 (d, J = 15.2 Hz, 1H), 4.04–3.89 (m, 1H), 3.87 (d, J = 9.5 Hz, 1H), 3.77 (d, J = 7.6 Hz, 1H), 3.59 (s, 1H), 3.16 (d, J = 11.9 Hz, 3H), 2.89 (ddd, J = 23.5, 13.7, 4.5 Hz, 1H), 2.68 (ddd, J = 28.5, 13.7, 9.6 Hz, 1H), 2.23 (d, J = 4.2 Hz, 3H). ^{13}C NMR (150 MHz, DMSO- d_6) δ 170.78, 170.20, 167.30, 161.46 (dd, J = 245.7, 13.0 Hz), 161.30, 159.21, 142.38, 135.20, 135.24, 134.24, 130.00 (d, J = 7.4 Hz), 129.72, 129.45 (d, J = 8.0 Hz), 129.16, 125.94, 125.91, 123.90, 123.80, 121.67, 121.56, 115.76, 115.64, 115.40, 115.32, 115.32, 115.13, 113.72, 113.64, 112.36, 112.43, 112.32, 112.24, 111.46, 108.56, 102.40, 102.26, 55.89, 51.54, 49.92, 49.16, 37.72, 37.32, 30.31, 15.32. ESI-MS: m/z 637.42 [M – 1] $^-$, C₃₇H₃₆F₂N₄O₄ [638.27].

(S)-2-(2-(N-benzyl-2-(naphthalen-2-yl)acetamido)acetamido)-3-(3,5-difluorophenyl)-N-(4-methoxyphenyl)-N-methylpropanamide (**I-22**):

Light-yellow solid, yield 10.50%, mp: 46–48 °C. ¹H NMR (600 MHz, DMSO-*d*₆) δ 8.53 (d, *J* = 8.3 Hz, 1H), 7.89 (s, 1H), 7.83 (dd, *J* = 15.8, 8.8 Hz, 2H), 7.63 (s, 1H), 7.52–7.45 (m, 2H), 7.38–7.32 (m, 2H), 7.29 (dd, *J* = 8.0, 6.1 Hz, 3H), 7.26–7.23 (m, 1H), 7.15 (dd, *J* = 21.0, 7.2 Hz, 3H), 7.07–6.97 (m, 3H), 6.56–6.46 (m, 2H), 4.60 (td, *J* = 9.2, 8.1, 4.6 Hz, 1H), 4.34 (dd, *J* = 133.6, 15.0 Hz, 2H), 4.00–3.92 (m, 2H), 3.87 (d, *J* = 17.5 Hz, 1H), 3.80 (d, *J* = 8.4 Hz, 3H), 3.70 (s, 1H), 3.15 (d, *J* = 19.0 Hz, 3H), 2.89 (ddd, *J* = 27.5, 13.7, 4.3 Hz, 1H), 2.72–2.64 (m, 1H). ¹³C NMR (100 MHz, DMSO-*d*₆) δ 171.70, 170.81, 168.18, 163.80, 163.67, 161.22, 159.22, 138.01, 135.85, 133.91, 133.42, 132.25, 129.21, 129.14, 128.84, 128.48, 128.40, 128.15, 127.94, 127.89, 127.80, 127.57, 127.41, 126.49, 126.01, 115.34, 115.25, 112.54, 112.30, 102.53, 55.94, 55.91, 51.49, 49.77, 49.56, 47.60, 37.82, 37.31. ESI-MS: *m/z* 637.38 [M + 1]⁺, C₃₈H₃₅F₂N₃O₄ [636.05].

(S)-4-(2-((3-(3,5-difluorophenyl)-1-((4-methoxyphenyl)(methyl)amino)-1-oxopropan-2-yl)amino)-2-oxoethyl)(4-fluorobenzyl)amino)-2-oxoethylphenyl boronic acid (**I-23**):

White solid, yield 12.0%, mp: 123.6–125.8 °C. ¹H NMR (400 MHz, DMSO-*d*₆) δ 8.52 (d, *J* = 8.2 Hz, 1H), 7.98 (s, 2H), 7.73 (d, *J* = 7.6 Hz, 2H), 7.27 (d, *J* = 8.5 Hz, 2H), 7.23–7.17 (m, 3H), 7.14–7.11 (m, 3H), 7.07–6.98 (m, 3H), 6.53 (d, *J* = 7.1 Hz, 2H), 4.63–4.50 (m, 1H), 4.42 (d, *J* = 14.8 Hz, 1H), 4.20 (d, *J* = 15.0 Hz, 1H), 3.92 (dd, *J* = 16.7, 6.9 Hz, 1H), 3.81 (s, 3H), 3.75 (d, *J* = 7.6 Hz, 1H), 3.52 (s, 2H), 3.15 (d, *J* = 11.2 Hz, 3H), 2.90 (dt, *J* = 17.7, 8.8 Hz, 1H), 2.75–2.61 (m, 1H). ¹³C NMR (150 MHz, DMSO-*d*₆) δ 171.69, 170.79, 168.11, 163.35 (d, *J* = 13.3 Hz), 161.92 (dd, *J* = 243.3, 17.8 Hz), 161.72 (d, *J* = 13.3 Hz), 159.24, 142.53, 142.47, 137.90, 135.86, 134.56, 134.49, 134.22, 130.22 (d, *J* = 8.1 Hz), 129.50 (d, *J* = 8.2 Hz), 129.14, 128.75, 128.69, 115.81 (d, *J* = 21.3 Hz), 115.49 (d, *J* = 21.3 Hz), 115.34, 115.29, 112.39 (d, *J* = 24.4 Hz), 102.47, 102.30, 55.93, 51.42, 49.85, 49.05, 47.65, 37.79, 37.42. ESI-MS: *m/z* 648.52 [M + 1]⁺, C₃₄H₃₃BF₃N₃O₆. [647.24].

4.2. In Vitro Anti-HIV Assay

The evaluation of the antiviral activity of the compounds against HIV in MT-4 cells was performed using the MTT assay as described below. Stock solutions (10 × final concentration) of test compounds were added in 25 µL volumes to two series of triplicate wells to allow simultaneous evaluation of their effects on mock- and HIV-infected cells at the beginning of each experiment. Serial 5-fold dilutions of test compounds were made directly in flat-bottomed 96-well microtiter trays using a Biomek 3000 robot (Beckman Instruments, Fullerton, CA). Untreated HIV- and mock-infected cell samples were included as controls. HIV stock (50 mL) at 100–300 CCID₅₀ (50% cell culture infectious doses) or culture medium was added to either the infected or mock-infected wells of the microtiter tray. Mock-infected cells were used to evaluate the effects of the test compound on uninfected cells to assess the test compounds' cytotoxicity. Exponentially growing MT-4 cells were centrifuged for 5 min at 220 g, and the supernatant was discarded. The MT-4 cells were resuspended at 6 × 10⁵ cells/mL, and 50 µL volumes were transferred to the microtiter tray wells. Five days after infection, the viability of mock- and HIV-infected cells was examined spectrophotometrically using the MTT assay. The MTT assay is based on the reduction of yellow-colored 3-(4,5-dimethylthiazol-2-yl)-2,5-diphenyltetrazolium bromide (MTT) (Acros Organics) by mitochondrial dehydrogenase activity in metabolically active cells to a blue-purple formazan that can be measured spectrophotometrically. The absorbances were read in an eight-channel computer-controlled photometer (Infinite M1000, Tecan) at two wavelengths (540 and 690 nm). All data were calculated using the median absorbance value of three wells. The 50% cytotoxic concentration (CC₅₀) was defined as the concentration of the test compound that reduced the absorbance (OD₅₄₀) of the mock-infected control sample by 50%. The concentration achieving 50% protection against the cytopathic effect of the virus in infected cells was defined as the 50% effective concentration (EC₅₀).

4.3. Binding to CA Proteins Analysis via Surface Plasmon Resonance (SPR)

The CA hexamer was generated by introducing mutations at the following sites: A14C, E45C, W184A, and M185A through site-directed mutagenesis (Stratagene). While the A14C and E45C mutations stabilized the CA hexamer, the W184A and M185A prevented further oligomerization of hexamers into CA cones and tubes. All binding assays were performed on a ProteOn XPR36 SPR Protein Interaction Array System (Bio-Rad Laboratories, Hercules, CA, USA). The instrument temperature was set at 25 °C for all kinetic analyses. ProteOn GLH sensor chips were preconditioned with two short pulses each (10 s) of 50 mM NaOH, 100 mM HCl, and 0.5% sodium dodecyl sulfide. Then, the system was equilibrated with PBS-T buffer (20 mM sodium phosphate, 150 mM NaCl, and 0.005% polysorbate 20, pH 7.4). The surface of a GLH sensorchip was activated with a 1:100 dilution of a 1:1 mixture of 1-ethyl-3-(3-dimethylaminopropyl) carbodiimide hydrochloride (0.2 M) and sulfo-*N*-hydroxysuccinimide (0.05 M). Immediately after chip activation, the HIV-1 NL4-3 capsid protein constructs, purified as in the study by Xu et al. [40], were prepared at a concentration of 100 µg/mL in 10 mM sodium acetate, pH 5.0, and injected across ligand and flow channels for 5 min at a flow rate of 30 µL/min. Then, after unreacted protein had been washed out, excess active ester groups on the sensor surface were capped by a 5 min injection of 1 M ethanolamine HCl (pH 8.0) at a flow rate of 5 µL/min. A reference surface was similarly created by immobilizing a nonspecific protein (IgG b12 anti HIV-1 gp120; obtained through the NIH AIDS Reagent Program, Division of AIDS, NIAID, NIH: Anti-HIV-1 gp120 Monoclonal (IgG1 b12) from Dr. Dennis Burton and Carlos Barbas) and was used as a background to correct nonspecific binding.

To prepare a compound for direct binding analysis, compound stock solutions, along with 100% DMSO, totaling 30 µL were made to a final volume of 1 mL by addition of sample preparation buffer (PBS, pH 7.4). Preparation of analyte in this manner ensured that the concentration of DMSO was matched with that of the running buffer with 3% DMSO. Serial dilutions were then prepared in the running buffer (PBS, 3% DMSO, 0.005% polysorbate 20, pH 7.4) and injected at a flow rate of 100 µL/min, for a 1 min association phase, followed by up to a 5 min dissociation phase using the “one shot kinetics” capability of the Proteon instrument [41]. Data were analyzed using the ProteOn Manager Software version 3.0 (Bio-Rad). The responses from the reference flow cell were subtracted to account for the nonspecific binding and injection artifacts. Experimental data were fitted to a simple 1:1 binding model (where applied). The average kinetic (association [k_a] and dissociation [k_d] rates) and equilibrium parameters generated from 3 replicates were used to define the on- and off-rates and equilibrium dissociation constant (K_D). Please refer to the Supplementary Document for more details.

4.4. Molecular Docking and MD Simulation

The methodology followed in this study (molecular docking and MD simulation) was taken from our previous work [42]. There are reports available on structural similarities of NTD of HIV-1 CA (PDB code: 3H4E) and truncated HIV-2 CA NTD (PDB code: 2WLV). As “HIV-1 is more virulent than HIV-2” as well as the unavailability of the complete structure of HIV-2 CA protein, we selected HIV-1 CA as a target protein [43]. In order to further verify the accuracy of the docking observations, complexes of compound **I-19** and **PF-74** with capsid protein were selected for extensive 100 ns MD simulation. The structure of the gag-polyprotein (PDB: 5TSX, 5HGL) was obtained from the RCSB website (<https://www.rcsb.org>) for ligand-protein complex interaction analysis. The Schrödinger software (Desmond software, NY, USA) was used to perform the computational work. The structures were prepared prior to docking to remove structural errors. The compounds **I-19** and **PF-74** were prepared by the Ligprep tool prior to docking. Schrödinger suite inbuilt Epik module was used to predict the ionization states of all compounds at pH 7 ± 2 and tautomers generated. This in silico study was carried out under the OPLS2005 forcefield. Site-specific molecular docking of both compounds against HIV-1 capsid protein was performed at XP precision using the Glide module of Schrödinger suite. The binding site of

capsid protein (PDB: 5TSX) was defined in reference to PDB: 5HGL. The Van der Waals radii scaling factor was 0.8, and the partial charge cutoff was set to 0.15. Both complexes were introduced into the Desmond software to study the binding stability of both compounds within their respective complex. These complexes were solvated in a TIP3P water model, and Na⁺ ions were added to neutralize both complexes. The stereo-chemical geometry of 5TSX protein residues was measured by a Ramachandran map by procheck. Please refer to the Supplementary Document for more details.

Supplementary Materials: Supplementary material includes materials and methods for MD and SPR. MS, ¹H-NMR and ¹³C-NMR spectra for compounds [1–7].

Author Contributions: Conceptualization, X.J. (Xiangkai Ji) and J.L.; methodology, X.J. (Xiangkai Ji) and X.J. (Xiangyi Jiang); software, P.P.S. and B.R.; validation, C.P., X.J. (Xiangkai Ji), E.D.C., S.C. and A.D.; formal analysis, C.L., Z.G. and L.H.; investigation, X.J. (Xiangkai Ji) and D.K.; resources, X.J. (Xiangkai Ji) and X.L.; data curation, X.J. (Xiangkai Ji) and J.L.; writing—original draft preparation, X.J. (Xiangkai Ji); writing—review and editing, X.J. (Xiangkai Ji), X.J. (Xiangyi Jiang), A.D. and P.Z.; visualization, X.J. (Xiangkai Ji); supervision, X.L. and P.Z.; project administration, X.L. and P.Z.; funding acquisition, X.L. and P.Z. All authors have read and agreed to the published version of the manuscript.

Funding: This research was funded by the National Natural Science Foundation of China [(NSFC Nos. 82173677, 81773574)], the Key Project of NSFC for International Cooperation [(No. 81420108027)], the Shandong Provincial Key Research and Development Project [(No. 2019JZZY021011)], the Science Foundation for Outstanding Young Scholars of Shandong Province (ZR2020JQ31) and NIH/NIAID grant R01AI150491 (Cocklin, PI, Salvino, Coel). BR is highly grateful to Department of Science & Technology for financial support (DST/INT/BRICS/COVID-19/2020-Part-1).

Institutional Review Board Statement: Not applicable.

Informed Consent Statement: Not applicable.

Data Availability Statement: Not applicable.

Conflicts of Interest: The authors declare no conflict of interest.

Sample Availability: Samples of the compounds are available from the authors.

References

1. De Clercq, E. Antivirals: Past, present and future. *Biochem. Pharmacol.* **2013**, *85*, 727–744. [[CrossRef](#)]
2. Smith, R.A.; Wu, V.H.; Zavala, C.G.; Raugi, D.N.; Ba, S.; Seydi, M.; Gottlieb, G.S. In vitro antiviral activity of cabotegravir against HIV-2. *Antimicrob. Agents Chemother.* **2018**, *62*, e01299-18. [[CrossRef](#)] [[PubMed](#)]
3. Menéndez-Arias, L. Molecular basis of human immunodeficiency virus type 1 drug resistance: Overview and recent developments. *Antiviral Res.* **2013**, *98*, 93–120. [[CrossRef](#)] [[PubMed](#)]
4. Lamoel, A.; Yaniv, O.; Berger, O.; Bacharach, E.; Gazit, E.; Frolow, F. A triclinic crystal structure of the carboxy-terminal domain of HIV-1 capsid protein with four molecules in the asymmetric unit reveals a novel packing interface. *Acta Crystallogr. Sect. F Struct. Biol. Cryst. Commun.* **2013**, *69 Pt 6*, 602–606.
5. Chen, B. HIV capsid assembly, mechanism, and structure. *Biochemistry* **2016**, *55*, 2539–2552. [[CrossRef](#)]
6. Chen, N.Y.; Zhou, L.; Gane, P.J.; Opp, S.; Ball, N.J.; Nicastro, G.; Zufferey, M.; Buffone, C.; Luban, J.; Selwood, D.; et al. HIV-1 capsid is involved in post-nuclear entry steps. *Retrovirology* **2016**, *13*, 28. [[CrossRef](#)]
7. Lahaye, X.; Satoh, T.; Gentili, M.; Cerboni, S.; Conrad, C.; Hurbain, I.; El Marjou, A.; Lacabaratz, C.; Lelièvre, J.D.; Manel, N. The capsids of HIV-1 and HIV-2 determine immune detection of the viral cDNA by the innate sensor cGAS in dendritic cells. *Immunity* **2013**, *39*, 1132–1142. [[CrossRef](#)] [[PubMed](#)]
8. Yamashita, M.; Engelman, A.N. Capsid-dependent host factors in HIV-1 infection. *Trends Microbiol.* **2017**, *25*, 741–755. [[CrossRef](#)] [[PubMed](#)]
9. Pornillos, O.; Ganser-Pornillos, B.K.; Kelly, B.N.; Hua, Y.; Whitby, F.G.; Stout, C.D.; Sundquist, W.I.; Hill, C.P.; Yeager, M. X-ray structures of the hexameric building block of the HIV capsid. *Cell* **2009**, *137*, 1282–1292. [[CrossRef](#)]
10. Zhao, G.; Perilla, J.R.; Yufenyuy, E.L.; Meng, X.; Chen, B.; Ning, J.; Ahn, J.; Gronenborn, A.M.; Schulten, K.; Aiken, C.; et al. Mature HIV-1 capsid structure by cryo-electron microscopy and all-atom molecular dynamics. *Nature* **2013**, *497*, 643–646. [[CrossRef](#)]
11. Pornillos, O.; Ganser-Pornillos, B.K.; Yeager, M. Atomic-level modelling of the HIV capsid. *Nature* **2011**, *469*, 424–427. [[CrossRef](#)] [[PubMed](#)]

12. Tang, C.; Loeliger, E.; Kinde, I.; Kyere, S.; Mayo, K.; Barklis, E.; Sun, Y.; Huang, M.; Summers, M.F. Antiviral inhibition of the HIV-1 capsid protein. *J. Mol. Biol.* **2003**, *327*, 1013–1020. [[CrossRef](#)]
13. Kelly, B.N.; Kyere, S.; Kinde, I.; Tang, C.; Howard, B.R.; Robinson, H.; Sundquist, W.I.; Summers, M.F.; Hill, C.P. Structure of the antiviral assembly inhibitor CAP-1 complex with the HIV-1 CA protein. *J. Mol. Biol.* **2007**, *373*, 355–366. [[CrossRef](#)] [[PubMed](#)]
14. Fader, L.D.; Bethell, R.; Bonneau, P.; Bös, M.; Bousquet, Y.; Cordingley, M.G.; Coulombe, R.; Deroy, P.; Faucher, A.M.; Gagnon, A.; et al. Discovery of a 1,5-dihydrobenzo[*b*][1,4]diazepine-2,4-dione series of inhibitors of HIV-1 capsid assembly. *Bioorg. Med. Chem. Lett.* **2011**, *21*, 398–404. [[CrossRef](#)] [[PubMed](#)]
15. Fader, L.D.; Landry, S.; Goulet, S.; Morin, S.; Kawai, S.H.; Bousquet, Y.; Dion, I.; Hucke, O.; Goudreau, N.; Lemke, C.T.; et al. Optimization of a 1,5-dihydrobenzo[*b*][1,4]diazepine-2,4-dione series of HIV capsid assembly inhibitors 2: Structure-activity relationships (SAR) of the C3-phenyl moiety. *Bioorg. Med. Chem. Lett.* **2013**, *23*, 3401–3405. [[CrossRef](#)] [[PubMed](#)]
16. Lemke, C.T.; Titolo, S.; von Schwedler, U.; Goudreau, N.; Mercier, J.F.; Wardrop, E.; Faucher, A.M.; Coulombe, R.; Banik, S.S.; Fader, L.; et al. Distinct effects of two HIV-1 capsid assembly inhibitor families that bind the same site within the N-terminal domain of the viral CA protein. *J. Virol.* **2012**, *86*, 6643–6655. [[CrossRef](#)]
17. Sun, L.; Dick, A.; Meuser, M.E.; Huang, T.; Zalloum, W.A.; Chen, C.H.; Cherukupalli, S.; Xu, S.; Ding, X.; Gao, P.; et al. Design, synthesis, and mechanism study of benzenesulfonamide-containing phenylalanine derivatives as novel HIV-1 capsid inhibitors with improved antiviral activities. *J. Med. Chem.* **2020**, *63*, 4790–4810. [[CrossRef](#)]
18. Link, J.O.; Rhee, M.S.; Tse, W.C.; Zheng, J.; Somoza, J.R.; Rowe, W.; Begley, R.; Chiu, A.; Mulato, A.; Hansen, D.; et al. Clinical targeting of HIV capsid protein with a long-acting small molecule. *Nature* **2020**, *584*, 614–618. [[CrossRef](#)]
19. Blair, W.S.; Pickford, C.; Irving, S.L.; Brown, D.G.; Anderson, M.; Bazin, R.; Cao, J.; Ciaramella, G.; Isaacson, J.; Jackson, L.; et al. HIV capsid is a tractable target for small molecule therapeutic intervention. *PLoS Pathog.* **2010**, *6*, e1001220. [[CrossRef](#)]
20. Xu, J.P.; Francis, A.C.; Meuser, M.E.; Mankowski, M.; Ptak, R.G.; Rashad, A.A.; Melikyan, G.B.; Cocklin, S. Exploring modifications of an HIV-1 capsid inhibitor: Design, synthesis, and mechanism of action. *J. Drug Des. Res.* **2018**, *5*, 1070.
21. Meuser, M.E.; Reddy, P.A.N.; Dick, A.; Maurancy, J.M.; Salvino, J.M.; Cocklin, S. Rapid optimization of the metabolic stability of a human immunodeficiency virus type-1 capsid inhibitor using a multistep computational workflow. *J. Med. Chem.* **2021**, *64*, 3747–3766. [[CrossRef](#)]
22. Vernekar, S.K.V.; Sahani, R.L.; Casey, M.C.; Kankanala, J.; Wang, L.; Kirby, K.A.; Du, H.; Zhang, H.; Tedbury, P.R.; Xie, J.; et al. Toward structurally novel and metabolically stable HIV-1 capsid-targeting small molecules. *Viruses* **2020**, *12*, 452. [[CrossRef](#)]
23. Marcelin, A.G.; Charpentier, C.; Jary, A.; Perrier, M.; Margot, N.; Callebaut, C.; Calvez, V.; Descamps, D. Frequency of capsid substitutions associated with GS-6207 in vitro resistance in HIV-1 from antiretroviral-naïve and -experienced patients. *J. Antimicrob. Chemother.* **2020**, *75*, 1588–1590. [[CrossRef](#)] [[PubMed](#)]
24. Wang, L.; Casey, M.C.; Vernekar, S.K.V.; Do, H.T.; Sahani, R.L.; Kirby, K.A.; Du, H.; Hachiya, A.; Zhang, H.; Tedbury, P.R.; et al. Chemical profiling of HIV-1 capsid-targeting antiviral PF74. *Eur. J. Med. Chem.* **2020**, *200*, 112427. [[CrossRef](#)] [[PubMed](#)]
25. Wu, G.; Zalloum, W.A.; Meuser, M.E.; Jing, L.; Kang, D.; Chen, C.H.; Tian, Y.; Zhang, F.; Cocklin, S.; Lee, K.H.; et al. Discovery of phenylalanine derivatives as potent HIV-1 capsid inhibitors from click chemistry-based compound library. *Eur. J. Med. Chem.* **2018**, *158*, 478–492. [[CrossRef](#)]
26. Bhattacharya, A.; Alam, S.L.; Fricke, T.; Zdrozny, K.; Sedzicki, J.; Taylor, A.B.; Demeler, B.; Pornillos, O.; Ganser-Pornillos, B.K.; Diaz-Griffero, F.; et al. Structural basis of HIV-1 capsid recognition by PF74 and CPSF6. *Proc. Natl. Acad. Sci. USA* **2014**, *111*, 18625–18630. [[CrossRef](#)]
27. Bester, S.M.; Wei, G.; Zhao, H.; Adu-Ampratwum, D.; Iqbal, N.; Courouble, V.V.; Francis, A.C.; Annamalai, A.S.; Singh, P.K.; Shkriabai, N.; et al. Structural and mechanistic bases for a potent HIV-1 capsid inhibitor. *Science* **2020**, *370*, 360–364. [[CrossRef](#)]
28. Jiang, X.; Wu, G.; Zalloum, W.A.; Meuser, M.E.; Dick, A.; Sun, L.; Chen, C.H.; Kang, D.; Jing, L.; Jia, R.; et al. Discovery of novel 1,4-disubstituted 1,2,3-triazole phenylalanine derivatives as HIV-1 capsid inhibitors. *RSC Adv.* **2019**, *9*, 28961–28986. [[CrossRef](#)] [[PubMed](#)]
29. Wang, L.; Casey, M.C.; Vernekar, S.K.V.; Sahani, R.L.; Kirby, K.A.; Du, H.; Zhang, H.; Tedbury, P.R.; Xie, J.; Sarafianos, S.G.; et al. Novel PF74-like small molecules targeting the HIV-1 capsid protein: Balance of potency and metabolic stability. *Acta Pharm. Sin. B* **2021**, *11*, 810–822. [[CrossRef](#)]
30. Sun, L.; Huang, T.; Dick, A.; Meuser, M.E.; Zalloum, W.A.; Chen, C.H.; Ding, X.; Gao, P.; Cocklin, S.; Lee, K.H.; et al. Design, synthesis and structure-activity relationships of 4-phenyl-1H-1,2,3-triazole phenylalanine derivatives as novel HIV-1 capsid inhibitors with promising antiviral activities. *Eur. J. Med. Chem.* **2020**, *190*, 112085. [[CrossRef](#)]
31. Clas, S.D.; Sanchez, R.I.; Nofsinger, R. Chemistry-enabled drug delivery (prodrugs): Recent progress and challenges. *Drug Discov. Today* **2014**, *19*, 79–87. [[CrossRef](#)] [[PubMed](#)]
32. Suryanarayana Birudukota, N.V.; Franke, R.; Hofer, B. An approach to “escape from flatland”: Chemo-enzymatic synthesis and biological profiling of a library of bridged bicyclic compounds. *Org. Biomol. Chem.* **2016**, *14*, 3821–3837. [[CrossRef](#)] [[PubMed](#)]
33. Liu, M.; Quinn, R.J. Fragment-based screening with natural products for novel anti-parasitic disease drug discovery. *Expert. Opin. Drug Discov.* **2019**, *14*, 1283–1295. [[CrossRef](#)] [[PubMed](#)]
34. Jiang, X.; Huang, B.; Olotu, F.A.; Li, J.; Kang, D.; Wang, Z.; De Clercq, E.; Soliman, M.E.S.; Pannecouque, C.; Liu, X.; et al. Exploiting the tolerant region I of the non-nucleoside reverse transcriptase inhibitor (NNRTI) binding pocket. Part 2: Discovery of diarylpyrimidine derivatives as potent HIV-1 NNRTIs with high Fsp(3) values and favorable drug-like properties. *Eur. J. Med. Chem.* **2021**, *213*, 113051. [[CrossRef](#)] [[PubMed](#)]

35. Lovering, F.; Bikker, J.; Humblet, C. Escape from flatland: Increasing saturation as an approach to improving clinical success. *J. Med. Chem.* **2009**, *52*, 6752–6756. [[CrossRef](#)]
36. Yan, A.; Gasteiger, J. Prediction of aqueous solubility of organic compounds based on a 3D structure representation. *J. Chem. Inf. Comput. Sci.* **2003**, *43*, 429–434. [[CrossRef](#)]
37. Dömling, A.; Ugi, I.I. Multicomponent reactions with isocyanides. *Angew. Chem. Int. Ed. Engl.* **2000**, *39*, 3168–3210. [[CrossRef](#)]
38. Rocha, R.O.; Rodrigues, M.O.; Neto, B.A.D. Review on the Ugi multicomponent reaction mechanism and the use of fluorescent derivatives as functional chromophores. *ACS Omega* **2020**, *5*, 972–979. [[CrossRef](#)]
39. Carnes, S.K.; Sheehan, J.H.; Aiken, C. Inhibitors of the HIV-1 capsid, a target of opportunity. *Curr. Opin. HIV AIDS* **2018**, *13*, 359–365. [[CrossRef](#)]
40. Xu, J.P.; Branson, J.D.; Lawrence, R.; Cocklin, S. Identification of a small molecule HIV-1 inhibitor that targets the capsid hexamer. *Bioorg. Med. Chem. Lett.* **2016**, *26*, 824–828. [[CrossRef](#)]
41. Bravman, T.; Bronner, V.; Lavie, K.; Notcovich, A.; Papalia, G.A.; Myszka, D.G. Exploring “one-shot” kinetics and small molecule analysis using the ProteOn XPR36 array biosensor. *Anal. Biochem.* **2006**, *358*, 281–288. [[CrossRef](#)] [[PubMed](#)]
42. Jiang, X.; Sharma, P.P.; Rathi, B.; Ji, X.; Hu, L.; Gao, Z.; Kang, D.; Wang, Z.; Xie, M.; Xu, S.; et al. Discovery of novel 1,2,4-triazole phenylalanine derivatives targeting an unexplored region within the interprotomer pocket of the HIV capsid protein. *J. Med. Virol.* **2022**. *ahead of print*. [[CrossRef](#)] [[PubMed](#)]
43. Miyazaki, Y.; Miyake, A.; Doi, N.; Koma, T.; Uchiyama, T.; Adachi, A.; Nomaguchi, M. Comparison of biochemical properties of HIV-1 and HIV-2 capsid proteins. *Front. Microbiol.* **2017**, *8*, 1082. [[CrossRef](#)] [[PubMed](#)]